Annu. Rev. Phys. Chem. 1989. 40: 291–326

TRANSITION METAL OXIDES[1]

C. N. R. Rao

Solid State and Structural Chemistry Unit, Indian Institute of Science, Bangalore 560012, India

INTRODUCTION

Transition metal oxides constitute probably one of the most interesting classes of solids, exhibiting a variety of structures and properties (1–3). The nature of metal--oxygen bonding can vary between nearly ionic to highly covalent or metallic. The unusual properties of transition metal oxides are clearly due to the unique nature of the outer *d*-electrons. The phenomenal range of electronic and magnetic properties exhibited by transition metal oxides is especially noteworthy. Thus, we find oxides with metallic properties (e.g. RuO_2, ReO_3, $LaNiO_3$) at one end of the range and oxides with highly insulating behavior (e.g. $BaTiO_3$) at the other. There are also oxides that traverse both these regimes with change of temperature, pressure, or composition (e.g. V_2O_3, $La_{1-x}Sr_xVO_3$). Interesting electronic properties also arise from charge density waves (e.g. $K_{0.3}MoO_3$), charge ordering (e.g. Fe_3O_4), and defect ordering (e.g. $Ca_2Mn_2O_5$, $Ca_2Fe_2O_5$). Oxides with diverse magnetic properties anywhere from ferromagnetism (e.g. CrO_2, $La_{0.5}Sr_{0.5}MnO_3$) to antiferromagnetism (e.g. NiO, $LaCrO_3$) are known. Many oxides possess switchable orientation states as in ferroelectric (e.g. $BaTiO_3$, $KNbO_3$) and ferroelastic [e.g. $Gd_2(MoO_4)_3$] materials. No discovery in solid state science has created as much sensation, however, as that of high-temperature superconductivity in cuprates (4). Although superconductivity in transition metal oxides has been known for some time, the highest T_c reached was around 13K; we now have oxides with T_cs in the region of 130K. The discovery of high T_c oxides has focused worldwide scientific attention on the chemistry of metal oxides and at the same time revealed how inadequate is our understanding of these fascinating materials.

[1] Contribution No. 595 from the Solid State and Structural Chemistry Unit.

0066–426X/89/1101–0291$02.00

In this article, I discuss some of the important aspects of the physical chemistry of transition metal oxides of current interest. In so doing, I had to be necessarily selective, as this is the first time that this vast topic has been reviewed here. I survey the electronic and magnetic properties as well as the structure of defect oxides and point out salient features of the different types of metal-insulator transition exhibited by metal oxides. The superconductivity of cuprates and other oxides is discussed at length in view of its timeliness. I briefly touch on some aspects related to synthesis and characterization before concluding the review with a look at future possibilities.

ELECTRONIC, MAGNETIC, AND RELATED PROPERTIES: AN OVERVIEW

In order to understand the relation between the structure and properties of oxides, it is necessary to have a proper description of the valence electrons. The two limiting descriptions of outer electrons in solids are the band theory and the ligand-field theory. In the band model, applicable to collective electron systems or systems in which the overlap between the orbitals of neighboring atoms is large, the energy U required to transfer a valence electron from one orbital to an other singly occupied orbital on an equivalent site is small compared to the bandwidth, W. In the ligand-field theory, applicable to localized electron situations, as in coordination compounds, U is large compared to W. When $U \approx W$, we have strongly correlated electrons in solids. Whereas outer s and p electrons interact strongly with neighboring atoms and are described by a collective-electron model, outer f electrons, which are tightly bound to the nuclei and well screened from the neighboring atoms, are best described by the localized electron model. Outer d electrons have an intermediate character, as they are not screened from the neighboring atoms by outer core electrons. Because of this property, d electrons exhibit itinerant electron properties as well as localized electron properties in transition metal oxides. Electronic properties of even simple oxides such as CoO and NiO do not conform to the predictions of the elementary band theory; these monoxides, which should be metals because of the partially occupied bands, are actually insulators.

The unusual properties of transition metal oxides that distinguish them from the metallic elements and alloys, covalent semiconductors, and ionic insulators are due to several factors:

1. Oxides of d-block transition elements have narrow electronic bands, because of the small overlap between the metal d and the oxygen p

orbitals. The bandwidths are typically of the order of 1 or 2 eV (rather than 5 to 15 eV as in most metals).

2. Electron correlation effects play an important role, as expected because of the narrow electronic bands. The local electronic structure can be described in terms of atomic-like states [e.g. $Cu^{1+}(d^{10})$, $Cu^{2+}(d^9)$ and $Cu^{3+}(d^8)$ for Cu in CuO] as in the Heitler-London limit.
3. The polarizability of oxygen is also of importance. The divalent oxide ion, O^{2-}, does not exactly describe the state of oxygen, and configurations such as O^{1-} have to be included, especially in the solid state. This gives rise to polaronic and bipolaronic effects. Species such as O^{1-}, which are oxygen holes with a p^5 configuration instead of the filled p^6 configuration of O^{2-}, can be mobile and correlated.
4. Many transition metal oxides are not truly three-dimensional, but have low-dimensional features. For example, La_2CuO_4 and La_2NiO_4 with the K_2NiF_4 structure are two-dimensional compared to $LaCuO_3$ and $LaNiO_3$, which are three-dimensional perovskites. Because of the varied features of individual oxides, it has not been possible to establish satisfactory theoretical models for complex transition metal oxides.

Empirical approaches have been found to be convenient to describe the electronic structures and properties of transition metal oxides. Based on empirically derived criteria for cation-cation and cation-anion-cation overlaps, Goodenough (2) has attempted to rationalize the nature of *d*-electrons in metal oxides. In this approach, conceptual phase diagrams are constructed in terms of the transfer energy, b_{ij}, which is related to cation-cation separation or the covalent mixing parameter of the cation-anion orbitals. Simple rules have also been proposed based on considerations of cation-oxygen-cation overlap and cation-cation separation. The following is one such rule:

$$R_c^{3d} = 3.2 - 0.05m - 0.03(Z - Z_{Ti}) - 0.04S_i(S_i + 1)\ \text{Å}.$$

Here, R_c is the critical cation-cation separation, m the formal charge on the cation, Z the atomic number, and S_i the net atomic spin. Since the radial extension of the $4d$ and $5d$ orbitals is larger than that of the $3d$ orbitals, $R_c(5d) > R_c(4d) > R_c(3d)$. The covalent mixing parameter increases with m and shows a minimum where S is maximum; the cation-oxygen overlap integral is higher for an anion sp_σ orbital than for a p_π one. One-electron energy-level diagrams that take into account the most probable hybridization between the cationic and anionic orbitals are quite useful in understanding and predicting electronic properties. Such a diagram for ReO_3 would show that this oxide is metallic because of the partly filled π^* band.

In simple transition metal monoxides possessing the NaCl structure, we find a 180° cation-oxygen-cation interaction. Those monoxides with a cation-cation separation higher than a critical value are insulators. Thus, TiO, with a short cation-cation distance ($R < R_c$), is metallic and VO ($R \sim R_c$) is a semimetal. TiO is Pauli-paramagnetic while VO shows temperature-dependent susceptibility at low temperatures. The Neèl temperature increases in the order MnO, FeO, CoO, NiO, accompanying the increase in the cation-anion overlap. Non-stoichiometric $Mn_{1-x}O$ samples show spin-glass behavior. Oxygen-deficient EuO shows a sharp drop in resistivity and becomes metallic at around 50K. Stoichiometric EuO (which is ferromagnetic) shows a transition from an insulating state to a metallic state upon application of pressure because of the promotion of a $4f$ electron to the $5d$ conduction band.

In dioxides of transition metals possessing the rutile structure, 135° cation-oxygen-cation interaction is possible between corner-shared octahedra, and 90° cation-anion-cation interaction is possible between edge-shared octahedra; a cation-cation interaction can also occur in the c-direction. These oxides can therefore become metallic through cation-cation or cation-oxygen-cation interaction. Metal-metal bonding occurs in these oxides depending on the c/a ratio, and such oxides show monoclinic distortion (e.g. VO_2). Tetragonal VO_2 ($R < R_c$) is, however, metallic; WO_2 and MoO_2 ($R < R_c$) are also metallic. CrO_2, with the longest c/a ratio, is a metallic ferromagnet, since one of the d-electrons is in the π^* band formed through cation-anion-cation interaction.

Sesquioxides of the first row transition metals possessing the corundum structure exhibit interesting properties, e.g. Ti_2O_3 and V_2O_3 undergoing temperature-induced transitions from an insulating state to a metallic state. Cation-cation interactions in the basal plane, as well as cation-oxygen-cation (135° and 90°) interactions, play a role in bestowing such properties to these oxides. Fe_2O_3 exhibits the well-known first-order spin-flip transition (Morin transition).

ABO_3 perovskites ideally have 180° cation-oxygen-cation interactions of the B-site cation; cation-cation interaction is remote because of the large distance associated with the cube-face diagonal. The influence of the A cations on the B–O covalency is indirect. Figure 1 lists some important perovskites. Those with the same d-electron configurations are grouped together in the columns. In each column the entries are arranged in the order of decreasing cation-anion transfer energy, b. The *dotted lines* in Figure 1 representing $b_\Pi = b_m$ (b_m is the critical value for spontaneous magnetism), $b_\Pi = b_c$, and $b_\sigma = b_c$ (b_c is the critical value of the transfer energy) separate oxides exhibiting localized electron behavior from those with collective electron properties. Compounds in column 1 are insulators because the B

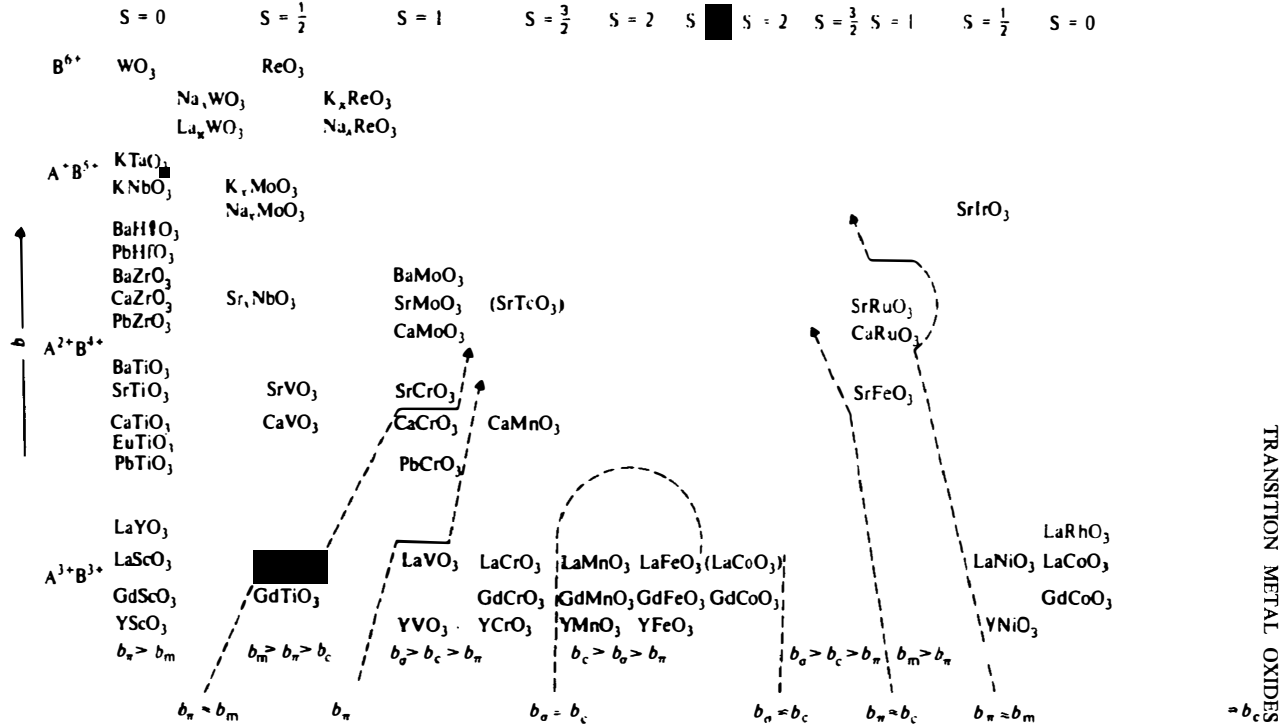

Figure 1 Perovskite oxides containing transition-metal ions in different spin configurations. Oxides are grouped into regions based on the transfer energy, b [following Goodenough (2)].

cations are of d^5 electron configuration. Most of the compounds in column 2 (spin $S = 1/2$) are metallic and Pauli paramagnetic; the line $b_\Pi = b_m$ separates $LaTiO_3$ from $GdTiO_3$ because $GdTiO_3$ is a semiconductor with a ferromagnetic Curie temperature (T_c) of 21K. $AMoO_3$ (A = Ca, Sr, Ba) and $SrCrO_3$ in the third column ($S = 1$) are metallic and Pauli paramagnetic. Other compounds in this column are semiconducting and antiferromagnetic. The line $b_\Pi = b_m$ separates the metallic, Pauli paramagnetic $SrCrO_3$ from $CaCrO_3$, which is an antiferromagnetic semimetal. The line $b_\Pi = b_c$ separates $PbCrO_3$ from $LaVO_3$ because the latter exhibits a crystallographic transition at a temperature lower than the Neèl temperature (T_N) characteristic of localized electrons. The region $b_m > b_\Pi > b_c$ appears to be narrow, as revealed by electrical, magnetic, and associated properties. Pressure experiments are valuable in the study of this region; thus, $dT_N/dP < 0$ in $CaCrO_3$ whereas $dT_N/dP > 0$ in $YCrO_3$ and $CaMnO_3$. Since increasing pressure increases b_Π (by decreasing lattice dimensions), $dT_N/dP > 0$ for $b_\Pi < b_c$ (localized behavior) and $dT_N/dP < 0$ for $b_m > b_x > b_c$ (collective behavior). Compounds in columns 4, 5, and 6 are antiferromagnetic insulators. Since intra-atomic exchange, given by $S(S+1)$, decreases the covalent mixing, the maxima in the curves $b_\pi = b_c$ and $b_\sigma = b_c$ corresponding to smallest values of b_Π and b_σ occur in the middle of the columns with $S = 5/2$. $LaFeO_3$ has a higher T_N than $LaCrO_3$ because of greater superexchange through σ bonding. The rare earth orthoferrites, which are antiferromagnetic insulators, exhibit parasitic ferromagnetism. The important contributions here are: (*a*) the Fe^{3+} spins canted in a common direction either by cooperative buckling of the oxygen octahedra or by anisotropic superexchange, and (*b*) canting of antiferromagnetic rare earth sublattice because of the interaction between the two sublattices.

$LaCoO_3$ is shown twice in Figure 1, both in $S = 2$ and $S = 0$ columns because Co^{3+} in this solid can have either the low-spin or the high-spin configuration. The compound exhibits a transition from a localized electron state to a collective electron state (metal-insulator transition) at ~1200K. In the ninth column of Figure 1, perovskites containing d^4 cations are placed. Of the three compounds in this column, $SrRuO_3$ is a ferromagnetic metal ($T_c = 160$K) and $CaRuO_3$ is antiferromagnetic ($T_N = 110$K) with a weak ferromagnetism. Since both the compounds have the same RuO_3 array, the change from ferromagnetic to antiferromagnetic coupling is of significance. $SrFeO_3$ is placed in the same column on the assumption that $Fe^{4+}(3d^4)$ is in the low-spin state, but there is reason to believe that Fe^{4+} in this oxide is in the high-spin state down to 4K. $CaFeO_3$, on the other hand, seems to undergo disproportionation of Fe^{4+} to Fe^{3+} and Fe^{5+} below 290K. In the next to the last column containing $S = 1/2$

B cations, metallic and Pauli paramagnetic $LaNiO_3$ should be separated from antiferromagnetic $YNiO_3$ to show that in $LaNiO_3$, $b_\sigma > b_m$, whereas in $YNiO_3$, $b_\sigma < b_m$. Similarly, in the last column, $LaCoO_3$ should be separated from $LaRhO_3$ because the latter is a narrow gap semiconductor with a filled $t_{2g}(\pi^*)$ band and an empty $e_g(\sigma^*)$ band.

Oxides such as $LaNi_{1-x}Mn_xO_3$, in which Mn^{2+} ions are present in a metallic oxide host, show spin-glass behavior (5); and these materials become insulators with an increase in x (6a,b). In $La_{1-x}Sr_xCoO_3$ and $La_{1-x}Sr_xMnO_3$, the material becomes metallic and ferromagnetic with an increase in x; the latter system is a well-known example of the Zener double exchange mechanism (6a,b).

Properties of a large number of perovskites have been compiled by Goodenough & Longo (7) and Nomura (8). Some of the oxide perovskites show superconductivity. One of the first oxides found to exhibit a reasonably high T_c (13K) was $BaPb_{1-x}Bi_xO_3$ (9). All the new high T_c cuprates possess perovskite-related structures. The perovskite motif occurs in many interesting classes of oxides; the K_2NiF_4 structure involving K F and $KNiF_3$ layers is the foremost. Properties of the oxides of K_2NiF_4 structure have been reviewed by Ganguly & Rao (10). In this structure, there is 180° B–O–B interaction in the basal plane and B–O–O–B interaction perpendicular to it. A tolerance factor can be defined for this structure similar to that in the perovskites. These two-dimensional oxides have electronic and magnetic properties that are distinctly different from those of the corresponding three-dimensional perovskites. Accordingly, $LaNiO_3$ is metallic and Pauli-paramagnetic whereas La_2NiO_4 exhibits two-dimensional antiferromagnetic ordering around 200K and a semiconductor-metal transition around 600K. While $LaCoO_3$ shows a spin-state transition of Co^{3+} and associated paramagnetism, La_2CoO_4 seems to exhibit antiferromagnetic ordering at fairly high temperatures (11). La_2CuO_4 is a low-resistivity oxide but not metallic, whereas $LaCuO_3$ is a metal; in La_2CuO_4 and other rare earth cuprates of this structure, copper has no magnetic moment. It has been suggested that La_2CuO_4 (orthorhombic-tetragonal transition $\sim$505K, $T_N \sim$ 290K) is in a quantum fluid
spins are ordered over long distances instantaneously, but no measurable time-averaged moment has been detected (12a). $La_2NiO_{4+\delta}$ (orthorhombic-tetragonal transition $\sim$240K, $T_N \sim$ 70K) shows strong two-dimensional magnetic correlations and also large in-plane spin velocities and in some ways has a behavior similar to that of La_2CuO_4 (12b). There are indications that $La_2NiO_{4+\delta}$ becomes superconducting at low temperatures just as $La_2CuO_{4+\delta}$ (12c,d).

In the $LaO(LaNiO_3)_n$ family, ($n = 1 = La_2NiO_4$, $n = \infty = LaNiO_3$), the electrical conductivity increases with increase in n (three-dimensional

character), becoming essentially metallic when $n = 3$ (13a). $SrRuO_3$ is a metallic ferromagnet, but Sr_2RuO_4 is a paramagnetic insulator.

A strict comparison of the properties of three- and two-dimensional oxides can be made only when the *d*-electron configuration of the transition metal ion, B, is the same. A comparative study of two such systems has been made with respect to their electrical and magnetic properties (13a,b). For example, members of the $La_{1-x}Sr_{1+x}CoO_4$ system are all paramagnetic semiconductors with a high activation energy for conduction, unlike $La_{1-x}Sr_xCoO_3$ ($x \geq 0.3$), which is metallic and ferromagnetic (6a,b). $La_{0.5}Sr_{1.5}CoO_4$ shows a magnetization of $0.5\mu_B$ at 0K (compared to $1.5\mu_B$ of $La_{0.5}Sr_{0.5}CoO_3$), but the high-temperature susceptibilities of the two systems are comparable. In $SrO(La_{0.5}Sr_{0.5}MnO_3)_n$, both magnetization and electrical conductivity increase with increase in n, approaching the value of the perovskite, $La_{0.5}Sr_{0.5}MnO_3$. $LaSrMn_{0.5}Ni_{0.5}(Co_{0.5})O_4$ shows no evidence of long-range ferromagnetic ordering, unlike the perovskite $LaMn_{0.5}Ni_{0.5}(Co_{0.5})O_3$; high-temperature susceptibility behavior of these two insulating systems is similar. $LaSr_{1-x}Ba_xNiO_4$ exhibits high electrical resistivity with the resistivity increasing proportionately with the magnetic susceptibility. High-temperature susceptibility of $LaSrNiO_4$ and $LaNiO_3$ are comparable. Susceptibility measurements show no evidence for long-range ordering in $LaSrFe_{1-x}Ni_xO_4$, unlike in $LaFe_{1-x}Ni_xO_3$ ($x \leq 0.35$), and the electrical resistivity of the former system is considerably higher.

Among the other interesting oxide families with the perovskite motif, mention should be made of the oxides of the Aurivillius family (14a,b), which possess the formula $(Bi_2O_2)^{2+}$ $(A_{n-1}B_nO_{3n+1})^{2-}$; typical members are $Bi_4Ti_3O_{12}$ ($n = 3$) and $BaBi_4Ti_4O_{15}$ ($n = 4$). The $A_nB_nO_{3n+2}$ formed by the Na–Ca–Nb–O system and the $A_{n+1}B_nO_{3n+1}$ family formed by the Sr–Ti–O and La–Ni–O systems (13a, 15) are of interest. Polytypic structures of perovskites wherein the AO_3 layer can be cubic or hexagonal with respect to the adjacent layers show large periodicities (e.g. $BaCrO_3$, $BaRuO_3$).

Oxide spinels AB_2O_4 are well-known magnetic systems exhibiting a variety of interesting properties (2, 3). Thus, ferrimagnetic $CoCr_2O_4$ has a conical spiral configuration. The cooperative Jahn-Teller effect shown by some of the spinels (e.g. $FeCr_2O_4$) is of considerable interest (16). Other oxides showing this effect are rare earth zircons (e.g. $TbVO_4$, $DyVO_4$) and $PrAlO_3$ (17, 18). In vandate spinels, $AV_2^{3+}O_4$, the *d*-electrons are localized when $2.88\ \text{Å} < R_{V-V} < 2.97\ \text{Å}$. Fe_3O_4, which is an inverse spinel, has been of much interest in the past several decades, and I discuss some aspects of this oxide further on in the review. It is noteworthy that the spinels $Li_{1-x}M_x^{2+}Ti_2O_4$ (M = Mg, Mn) and $Li_{1+x}Ti_{2-x}O_4$ show super-

conductivity (19a,b). In certain spinels such as $Ga_{0.8}Fe_{0.2}NiCrO_4$, spin-glass ordering with randomly frozen clusters has been noticed (20).

Oxide pyrochlores of the general formula $A_2B_2O_7$ show interesting electronic properties [see (21) for a review]. Ferromagnetic pyrochlores of rare earths have been described recently (22). A composition dependent metal-semiconductor transition has been found in $A_2(Ru_{2-x}A_x)O_{7-y}$ where A = Bi or Pb (23).

Transitions from the low-spin to the high-spin state of transition metal ions in oxide systems have been documented and models developed to explain the transitions (24). In $LaCoO_3$, low-spin Co^{3+} ions transform to the high-spin state upon increasing the temperature. Spin-state transitions have been found in niobium compounds as well (25). Quasi-two-dimensional oxides of K_2NiF_4 structures also exhibit such transitions (13a,b).

Hexagonal, cubic, and intergrowth bronzes formed by WO_3 with alkali, hydrogen, and other metals have been well-documented in the literature (26a–c). Of these, the intergrowth bronzes, in which strips of the hexagonal bronze intergrow with strips of WO_3, sometimes recurrently, are especially interesting. Electrical transport and other properties of WO_3 bronzes have been reviewed in the literature (27a,b). MoO_3 forms different varieties of bronzes (28): Blue bronzes of the type $A_{0.3}MoO_3$ (A = K, Tl, Rb), which are quasi-one-dimensional metals with charge density wave (CDW) instability; purple bronzes, $A_{0.9}Mo_6O_{17}$ (A = Na, K), which are quasi-two-dimensional metals with CDW instability; $Li_{0.9}Mo_6O_{17}$, which is one-dimensional and superconducting ($T_c \approx 2$K); red bronzes $A_{0.33}MoO_3$ (A = K, Tl, Rb), which are semiconducting; and $Li_{0.33}MoO_3$, which is violet and three-dimensional with low resistivity (29a,b). Hydrogen molybdenum bronzes, H_xMoO_3, of different compositions ($0 < x \leq 2.0$) with structures related to MoO_3, have been characterized (28). Conductivity measurements have been made on some of these hydrogen bronzes (30). Di- and mono-phosphate tungsten bronzes of the type $A_x(P_2O_4)_2(WO_3)_{2m}$ and $A_x(PO_2)_4(WO_3)_{2m}$ with A = Na, K, Rb, or Ba and possessing hexagonal tunnels, have been studied (31a–c). The tunnels may be empty, as in the monophosphate bronze $P_4W_8O_{32}$ ($m = 4$), or occupied, as in the diphosphate tungsten bronzes. Presence of defects and microstructures related to the adaptability of the phosphate groups to the WO_3 matrix have been examined. Anisotropic electronic properties of $CsP_8W_8O_{40}$, which has a unique structure, have been measured (32). Recently, layered alkali metal-MoO_3 bronzes as well as hexagonal bronzes of the type $K_yW_{1-x}Mo_xO_3$ have been prepared by a novel low-temperature reaction of the alkali metal iodide with the parent oxide (33).

Ferroics

Materials possessing two or more orientation states or domains that can be switched from one to another through the application of one or more appropriate forces belong to a general class called ferroics (34). In a ferromagnet, the orientation state of magnetization in domains is switched by the application of a magnetic field. In a ferroelastic, the direction of spontaneous strain in a domain is switched by the application of mechanical stress. In a ferroelectric, spontaneous electric polarization is altered by the application of an electric field. These three ferroics are primary ferroics, because they are governed by switchability of the properties. Metal oxides provide many examples of ferroics. $BaTiO_3$, $KNbO_3$ and the $Bi_2A_{n-1}B_nO_{3n+3}$ family of oxides are ferroelectric, whereas $PbZrO_3$ and $NaNbO_3$ are antiferroelectric.

Secondary ferroic properties occur as induced quantities, and the orientation states in these solids differ in the derivative quantities that characterize the induced effects (e.g. induced electric polarization characterized by dielectric susceptibility). Thus, $SrTiO_3$ is a secondary ferroic showing ferrobielectricity. NiO is ferrobimagnetic, whereas Cr_2O_3 is ferromagnetoelectric; Cr_2BeO_4 exhibits magnetoferroelectricity. Oxides such as $Pb(Mg_{1/3}Nb_{2/3})O_3$ with 10% $PbTiO_3$ are relaxor ferroelectrics, and $PbZr_{1-x}Ti_xO_3$ is a well-known electro-optic material.

Oxides exhibiting certain paired properties are especially interesting:

Ferroelectric-ferroelastic: $Gd_2(MoO_4)_3$, $KNbO_3$
Ferroelectric-ferromagnetic: $Bi_9Ti_3Fe_5O_{27}$
Ferroelectric-antiferromagnetic: $YMnO_3$, $HoMnO_3$
Antiferroelectric-antiferromagnetic: $BiFeO_3$
Ferroelectric-semiconducting: $SrTiO_3$, $YMnO_3$
Ferroelectric-superconducting: $SrTiO_3$

DEFECT OXIDES

It has been known since the 1920s that stoichiometric FeO does not fall in the stability range of iron (II) oxide. In fact, a large variety of oxides exhibit nonstoichiometry and wide homogeneity ranges. Nonstoichiometric oxides are mixed valent with nonintegral electron/atom ratios. Very few nonstoichiometric oxides, have, however point defects in high concentrations, and their structures can generally be understood in terms of defect ordering or complexation. New structural principles such as crystallographic shear and block structures have emerged in our efforts to understand defect oxides. $NbO_{2.4906}$, $NbO_{2.4167}$, $PrO_{1.714}$ and such solids are not to be merely considered as oxides with irrational ratios of the

constituent atoms, but as crystallographically well-defined $Nb_{53}O_{132}$, $Nb_{12}O_{29}$, and Pr_7O_{12}, etc. I briefl
encountered in trasition metal oxides (3, 18).

There is considerable evidence for superlattice ordering of point defects in many oxides (35, 36). Thus, TiO and VO, with ~20% vacancies, both have ordered defect structures. The high-temperature form of TiO with an averaged NaCl structure spans a wide range of compositions between $TiO_{0.65}$ and $TiO_{1.25}$ at 1770K (37). The low-temperature monoclinic form ($T < 1270$K) has a narrow composition range. The high-temperature form seems to have short-range order of its vacancies (38). The defect ordering in VO is quite different from that in TiO; VO and TiO are therefore immiscible. The superstructure in VO is formed at the oxygen-rich end, where the oxygen sublattice is filled and some V atoms occupy tetrahedral sites (e.g. $V_{52}O_{64}$, $V_{244}O_{320}$). Each tetrahedral cation has four vacant octahedral sites as nearest neighbors. The cluster so formed is topologically similar to the NaCl structure and gives rise to a $2\sqrt{2} \times 2\sqrt{2} \times 2$ superstructure. In the $V_{52}O_{64}$ superlattice, all the vacant octahedral sites are in the clusters, and there are no free vacancies (39).

Wüstite, which is always cation deficient, with the range $Fe_{0.85}O$–$Fe_{0.95}O$, is understood in terms of Koch-Cohen clusters, with the ratio of vacancies to tetrahedral Fe^{3+} of 3.25. Clusters with a ratio of ~2.5 are also found (40). Calculations show such clusters to be formed with a net lowering of free energy; binding energy of the 13 : 4 cluster is 2.1 eV (41). Starting from the rock salt structure, oxidation through the nonstoichiometric range may involve the following stages (36): isolated vacancies → dipolar associates → 4 : 1 clusters → 6 : 2, 8 : 3, 13 : 4 and other similar complex defect clusters → corner-shared 16 : 5 clusters → Fe_3O_4. Such clusters could be present in $Mn_{1-x}O$ as well. Although careful studies of Wüstite have been carried out by means of satellites in diffraction patterns and diffuse scattering, its constitution at high temperatures is still unclear, and no single cluster species seems to be able to explain the structure (42, 43). The thermodynamics of defects in $Mn_{1-x}O$ and $Fe_{1-x}O$ have been investigated in detail (44), but a real understanding will emerge only when we know the exact nature of defects. Energies of defect clusters in $M_{1-x}O$ (M = Mn, Fe, Co, or Ni) have also been calculated by using molecular orbital theory; extended defects are shown to be stable in MnO and FeO (45). A cluster component method (46) has been employed to understand defect ordering in $Fe_{1-x}O$ and $Mn_{1-x}O$.

In oxides with a fluor
anion-excess stoichiometries are known. In MO_{2-x} (M = Pr or Y-doped ZrO_2), Bevan clusters (47) are known to occur with tightly bound vacancies along ⟨111⟩ and 6-coordinated central ions with six 7-coordinated cations

surrounding them. Oxygen excess in UO_2 (e.g. U_4O_9) is understood in terms of Willis clusters of different types (2:1:2, 2:2:2, 3:4:2). Defect energy calculations have been performed (48), but we do not yet fully understand the nature of anion-excess fluo
defect formation in UO_2 and CeO_2 have been examined (44).

Point defects in oxides are eliminated by crystallographic shear (cs), and different types of cs planes are found in WO_3, MoO_3, and TiO_2 type structures, which give rise to homologous series of oxides (35, 49). An isolated cs plane or a random array of cs planes is referred to as the *Wadsley defect*. Crystallographic shear places can be regarded as translation modulations of the parent structure; the translation boundaries are cs planes. We have just begun to understand the mechanism of formation and ordering of cs planes. Elastic strain appears to play an important role in ordering. Both continuum and atom site models have been useful in illuminating this problem (49, 50).

Even slightly reduced rutile ($TiO_{1.997}$) shows the presence of cs planes. In slowly cooled samples of TiO_{2-x} ($0.0 < x \leq 0.01$), pairs of cs planes precipitate and separate subsequently (51). Novel {100} platelet defects occur along with cs planes when $0 < x \leq 0.0035$, and this can be understood in terms of cationic interstitial defects (51). The extrinsic and/or intrinsic nature of extended defects has been analyzed in TiO_{2-x} and WO_{3-x} by drawing Burgers circuits directly onto electron micrographs (52). The defect structure of TiO_{2-x} has been discussed at some length in the light of experimental and theoretical results (53).

The structures of many oxides, especially those of Nb (e.g. $Nb_{12}O_{29}$, $Nb_{25}O_{62}$, Nb_2O_5), are best described as block structures resulting from the operation of two sets of nearly orthogonal crystallographic shear. These structures have been studied extensively by electron microscopy (54, 55). Point defects as well as Wadsley defects can occur in block structures.

A remarkable feature of the Ti_nO_{2n-1} ($n = 10$–14) system is that the ($\bar{1}21$) cs plane swings continuously through all possible orientations to ($\bar{1}32$), thus giving rise to ordered phases for any composition between $TiO_{1.900}$ and $TiO_{1.937}$. Such a continuous series of ordered structures, called *infinitely adaptive structures* (56), has been found in other systems (e.g. Ta_2O_5–WO_3). Elastic strain energy plays a crucial role in forming such structures (57). Another impressive solid state phenomenon found in oxides is that of recurrent intergrowth of two structurally related units, which gives rise to a new homologous series of materials. Some examples are $Bi_4A_{m+n-2}B_{m+n}O_{3(m+n)+6}$, formed by the intergrowth of two oxides of the formula $Bi_2A_{n-1}B_nO_{3n+3}$; intergrowth bronzes of the formula A_xWO_3; and $A_{n+1}B_nO_{3n+1}$ (A = Sr or La, B = Ti or Ni), formed by the intergrowth of AO, with different number of layers of ABO_3. Hexagonal barium

ferrites, $Ba_{2n+p}M_{2n}Fe_{12(n+p)}O_{22n+19p}$, where M = Zn, Ni, etc and with $n = 1$--47, are also examples of recurrent intergrowths structures. The subject of intergrowth structures has been discussed at some length recently (58a,b). It becomes difficult to distinguish recurrent intergrowths from infinitely adaptive structures in some instances. Disordered intergrowth of related members of a family of oxides is of common occurrence.

Perovskites form A-site vacancies commonly; the bronzes are well-known examples. B-site vacancies are not favored but are found in certain oxides with highly covalent B–O bonds and strong B–B interaction. Anion-deficient perovskites with vacancy ordering are of common occurrence (e.g. $Ca_2Fe_2O_5$, $CaMnO_{2.667}$). In $Ca_2Mn_2O_5$, the Mn ions are square-pyramidally coordinated, whereas in $Ca_2Fe_2O_5$, the Fe ions are alternately present in octahedral and tetrahedral sites. In $Ca_2Fe_{2-x}Mn_2O_5$, ordering of transition metal ions with octahedral, tetrahedral, and square-pyramidal coordinations has been found (59). Magnetic and crystal structures of such oxides have been examined, as typified by a recent study of Sr_2CoFeO_5 (60). Phases of the type $Ca_xLa_{1-x}FeO_{3-y}$, $CaTi_{1-x}Fe_xO_{3-y}$ and $CaFe_xMn_{1-x}O_{3-y}$ have been studied extensively (61a,b, 62). The defect structure of a novel oxygen-deficient 6H polytypic oxide, $BaMn_{1-x}Fe_xO_{3-d}$ has been studied (63). Structural features of $CaMnO_{3-x}$ over the $0 < x \leq 0.5$ range have also been studied (64), as has the dependence of the structure and the electronic state of $SrFeO_3$ on composition and temperature (65). Anion-excess stoichiometry in perovskite oxides is accommodated by A and B-site vacancies. The available experimental results on defect perovskites have been reviewed adequately (3, 66). Molecular orbital calculations by the method of moments have been carried out to understand the defect patterns in perovskites (67).

Oxide pyrochlores, $A_2B_2O_6O'$, can tolerate vacancies at the A and O′ sites, thus giving phases of the type $A_2B_2O_6\square$ or (ABO_3) and $A\square B_2O_6\square$ or AB_2O_6 ($\square$ = vacancy). Typical examples are $Tl_2Nb_2O_6$ and $Tl_2U_2O_6$ (21). Novel defect pyrochlores of the type $ABi_2B_5O_{16}$, where A = Cs, Rb and B = Ta, Nb have been described (68).

Oxides of the K_2NiF_4 structure such as La_2MO_4 (M = Co, Ni, Cu) generally seem to possess La-deficiency. Oxygen-deficient Ca_2MnO_4 can be topotactically reduced to $Ca_2MnO_{3.5}$ (69). $Ca_2FeO_{3.5}$ seems to have a different type of defect ordering compared to the manganese analogue (70). Oxygen-excess $La_2NiO_{4+\delta}$ has been examined recently (12b, 71).

MIXED VALENCE

Many transition metal compounds exhibit the phenomenon of mixed valence, wherein the metal is present in more than one oxidation state.

Properties of such compounds are generally determined by the rate of electron transfer between the different oxidation states. A classification of these compounds has been made on the basis of the valence delocalization coefficient, and their properties have been reviewed (3, 72). This type of mixed valence is different from that prevalent in rare-earth and actinide materials in which valence fluctuation, heavy fermion behavior, and superconductivity are found. Depending on the relative energies of the f^n configuration and the Fermi-level due to non-f electrons, three electronic regimes are distinguished: (*a*) the magnetic regime, (*b*) the Kondo regime, and (*c*) the fluctuating valence regime (73). EuO and SmS show valence fluctuation under pressure due to the promotion of an f-electron to the conduction band.

In mixed valent rare earth oxides of the type Pr_6O_{11}, Pr_7O_{12}, and Tb_4O_7 related to the fluorite structure, the electronic conductivity is proportional to the product $[M^{3+}][M^{4+}]$, since it is controlled by the hopping (diffusion) mechanism. The conductivity reaches a maximum when this product becomes a maximum, the point at which the sign of the charge carriers also changes from n- to p-type (74). Oxides of the type Ti_3O_5 and V_3O_5 undergo metal-insulator transitions whereas oxides of the type Co_3O_4 are insulators. The presence of more than one oxidation state is readily recognizable from the formula in certain oxides such as Fe_3O_4, Pb_3O_4, V_nO_{2n-1}, Ti_nO_{2n-1}, and Pr_6O_{11}, but this is not so in oxides such as $BaBiO_3$ and Sb_2O_4. The last two have Bi/Sb ions in 3+ and 5+ states. Even in oxides of the type $BaPbO_3$, mixed valence has been invoked (75). Metal ions in the lower oxidation state (2+ or 3+) can be leached out by acid dissolution from Pb_3O_4, Pr_6O_{11}, Tb_4O_7 and similar insulating oxides, thus leaving only the dioxides in the solid state.

Fe_3O_4, with the inverse spinel structure, undergoes a ferrimagnetic-paramagnetic transition around 850K and a transition associated with charge ordering (*Verwey transition*) around 123K. The latter transition and the electronic properties of the oxide through the transition have been a subject of much study. An entire issue of *Philosophical Magazine* (Vol. *B* 42, No. 10, 1980) was devoted to this topic. Yet there is considerable uncertainty about the transition and the mechanism of conduction (76a,b, 77). The transition is markedly dependent on stoichiometry, and becomes second-order at large stoichiometric deviations. Most of the data on transport properties seem to suggest a small polaron model. The observed entropy change $[(R \ln 2)/\text{mol } Fe_3O_4]$ suggests the presence of dimer units below the transition temperature. Randomization of the Fe^{3+} and Fe^{2+} ions from an ordered state seems to be too naive a description of this fascinating transition.

$Ln_{1-x}Sr_xCoO_3$ (Ln = La, Nd, etc) becomes metallic when $x \geq 0.3$, and

the itinerancy of the *d*-electrons is associated with ferromagnetism. Mössbauer studies clearly show that cobalt has an average oxidation state between 3+ and 4+ (78). The rate of electron transfer obviously determines the nature of mixed valency in such oxides. $MoFe_2O_4$ is another oxide with fast electron transfer, and hence it has an average oxidation state of +2.5 for iron (79). Many other oxides show such behavior (80–82).

METAL–NONMETAL TRANSITIONS

The band structure of a crystalline solid made up of an even number of electrons can be made to change over to a structure wherein the empty and filled bands cross or overlap due to a change in pressure or temperature or by suitable doping. Such band-overlap or crossover transitions are generally accompanied by change in crystal structure and, in some instances, magnetic ordering as well. The celebrated Mott transition can occur from a metallic to a nonmctallic state when the band-width decreases sufficiently that it becomes smaller than the intrasite electron-electron energy because of localization induced by electron correlation. Localization can also occur because of disorder, as in amorphous materials, thus giving rise to a M–NM transition (*Anderson transition*); in such a transition, the band-width becomes less than the width of the distribution of random site energies. In spite of voluminous work and a general agreement on model patterns, we have yet to understand fully this fascinating phenomenon, which occurs in many transition metal oxides.

In this section, I examine a few illustrative cases and models. Greater details are available in recent reviews of the subject (83–86). The different types of metal-nonmetal (M–NM) transitions found in metal oxides are the following:

1. Pressure-induced transitions, as in NiO, in which the pressure increases the wavefunction overlap between neighbors to induce a change from localized to itinerant behavior of electrons.
2. Transitions as in Fe_3O_4 involving charge-ordering.
3. Transitions as in $LaCoO_3$ that are initially induced because of the different spin configurations of the transition metal ion; electron transfer between the two spin states initiates a process that eventually renders the oxide metallic around 1200K.
4. Transitions as in EuO arising from the disappearance of spin polarization band-splitting effects when the ferromagnetic Curie temperature is reached.
5. Compositionally induced transitions, as in VO_x, $La_{1-x}Sr_xCoO_3$, and

$LaNi_{1-x}Mn_xO_3$, in which changes of band structure in the vicinity of the Fermi level are brought about by a change in composition or are due to disorder-induced localization.

6. Transitions in two-dimensional systems, such as La_2NiO_4, in which Ni–O–Ni interaction can only occur in the *ab* plane (unlike in the three-dimensional analogue in $LaNiO_3$).
7. Temperature-induced transitions in a large class of oxides such as Ti_2O_3, VO_2, and V_2O_3.

The last category, involving temperature-induced M–NM transitions, deserves some elaboration. In Ti_2O_3, a second-order transition occurs around 410K, accompanied by a gradual change in the rhombohedral *c/a* ratio and a 100-fold jump in conductivity; the oxide remains paramagnetic throughout. A simple band-crossing mechanism occurring with the change in the *c/a* ratio explains this transition. Accordingly, substitution of Ti by V up to 10% in Ti_2O_3 makes the system metallic; the *c/a* ratio of this metallic solid solution and the high-temperature phase of TiO_3 are similar. In VO_2, a first-order transition occurs around 340K, accompanied by a change in structure (monoclinic to tetragonal) and a 10,000-fold jump in conductivity; the material remains paramagnetic throughout. A crystal distortion model wherein a gap opens up in the low-temperature low-symmetry structure adequately explains the transition. Substitution of trivalent ions such as Cr^{3+} and Al^{3+} for vanadium in VO_2 leads to a complex phase diagram with at least two insulating phases whose properties are significantly different from those of the insulating phase of pure VO_2. These phases are now fairly well understood (87).

The N–NM transition in V_2O_3 and its alloys has been a subject of a large number of publications. Pure V_2O_3 undergoes a first-order transition (monoclinic-rhombohedral) at 150K accompanied by a 10 million-fold jump in conductivity and an antiferromagnetic-paramagnetic transition. Application of pressure makes V_2O_3 increasingly metallic, thus suggesting that it is near a critical region; accordingly, doping with Ti or Cr has a marked effect on the transition; the former has a positive pressure effect and the latter a negative pressure effect. V_2O_3 also shows a second-order transition around 400K with a small conductivity anomaly. Mere crystal distortion or magnetic ordering cannot explain the large conductivity jump at 150K. The current status of the V_2O_3 transition is best presented in terms of Figure 2.

The schematic diagrams in Figure 2 show several interesting features. In V_2O_3 (98.5%)–Cr_2O_3 (1.5%), there are three transitions as shown in Figure 2(*a*). In the 0–150K range, the alloy is an antiferromagnetic insulator (AFI). There is a sharp transformation to the paramagnetic metallic

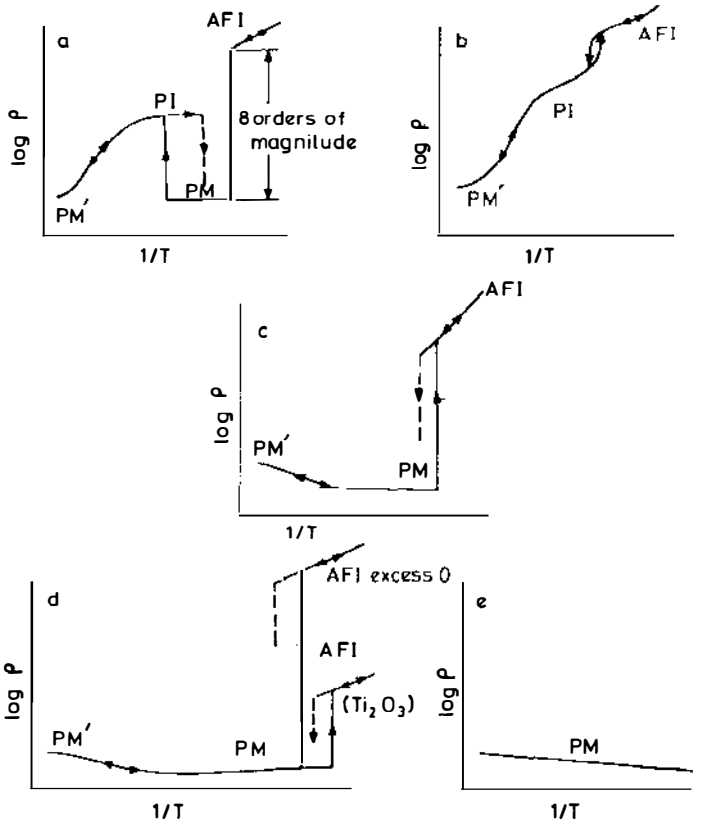

Figure 2 Schematic diagram depicting the changes of resistivity, P, with temperature, T, in the V_2O_3 alloy system as a function of dopants [from Honig & Spalek (85b)]. See text for a discussion of the different graphs.

state (PM), which prevails between 150 and 300K. At that point, another first-order transition transforms the oxide to a paramagnetic insulating state (PI). In the 300–1000K range, the resistivity gradually diminishes with increasing temperature, and beyond 650K, the alloy is in another paramagnetic metallic phase (PM′), which resembles the PM state. The three transitions are altered by minor changes through alloying. Electrical properties of the V_2O_3 (97%)–Cr_2O_3 (3%) are given in Figure 2(*b*). The PM phase is eliminated altogether, and the alloy goes directly from the AFI to the PI state via a sharp ($x > 0.03$) transition; this is followed by a gradual transition to the PM′ state. In pure V_2O_3, the resistivity exhibits a different pattern, as shown in Figure 2(*c*); there is a first-order

transition near 150K that links the AFI and PM phases. With increasing temperature in the 350–650K range, an anomalous rise in resistivity occurs and the undoped or lightly Cr_2O_3-doped V_2O_3 passes continuously from the PM to the PM′ state. Figure 2(*d*) gives the situation for V_2O_3 (99%)–Ti_2O_3 (1%) and for nonstoichiometric V_2O_3. The AFI–PM transition is shifted to lower temperature, and the resistivity discontinuity diminishes with increasing Ti/cation vacancy concentration. When the Ti content is increased beyond 5.5 or the vacancy concentration passes beyond 0.9, all transitions are eliminated and the PM phase is retained as shown in Figure 2(*e*). Below approximately 10–15K, however, the metallic phase transforms to an antiferromagnetic metal (AFM).

A variety of theoretical models have been proposed to explain M–NM transitions in metal oxides (83–85, 88). Here I briefly examine the mechanisms involving electron correlation and disorder. The phenomenon of correlation driven M–NM transition (*Mott transition*) was first pointed out by Mott (88). The simplest model for correlation effects in solids is that due to Hubbard (89). The possible phases of this model have been investigated in the one-body or Hartree-Fock approximation (90). The one electron density of states develops a gap when $(U/zt) > U_c \approx 1$. Here, z is number of near neighbors, t is the amplitude, and (U/zt) is dimensionless. The Hubbard gap increases with U, and at large U the material is an AFI whereas at small U it is a PM. The Hartree-Fock approximation is not satisfactory for M–NM transitions in which charge fluctuations, spin fluctuations, temperature, and mean-field have a comparable energy scale. Gutzwiller (91) introduced a different kind of approach that emphasizes local correlation effects and the relevance of this model to M–NM transitions due to correlation was pointed out by Brinkman & Rice (92). This model is satisfactory near the transition, but properties at $T \neq 0$ and of the insulating phase are not described, as spatial correlations have been completely ignored. Features such as orbital effects, electron-lattice interaction, Coulomb interaction, and disorder have also been ignored in this treatment.

Anderson (93) showed that when randomness exceeds a critical value, an electron locates itself around an appropriate potential fluctuation so that the state is spatially localized rather than extended, as in the case of weak disorder. The ratio W/Zt, where W is the spread of bandwidth, depends on the energy of the electron and on the dimensionality and connectivity of the lattice. Consequences of localization were clearly enunciated by Mott (94). A system becomes metallic or insulating depending on whether the states near the Fermi energy are extended or localized. With increasing disorder or decreasing Fermi energy, the mobility edge crosses the Fermi energy and the system becomes insulating. From this

model, one obtains the minimum metallic conductivity in three and two dimensions; the latter is a universal constant. The conductivity of a metal drops from σ_{min} to zero at the transition. There is considerable evidence for the change of the transport regime in disordered systems at σ_{min}. However, at very low temperatures close to critical disorder, it has been found that conductivity goes continuously to zero at the localization transition. A scaling theory of localization has been proposed to circumvent this difficulty (95). There are also theories that take into account interaction effects in disorder-driven M–NM transitions (96), but as yet no theories treat interaction or correlation effects sufficiently accurately to lead to the Mott transition and also include disorder effects.

The well-known criterion for the M–NM transition is that due to Mott. It states,

$$n^{1/3}a_H^* \approx 0.25$$

where a_H^* is the shallow state radius or atomic orbital size and n is the carrier density. This criterion is spectacularly successful (97) over a wide density range, although the transition is not discontinuous as predicted. It can be shown that the Anderson localization criterion, $\xi t = W$ (where ξ is the localization length), and the Hubbard criterion, $U \approx Zt$, are similar to Mott's criterion. In the Hubbard model, the incommensurate system is always metallic whereas the commensurate electronic system exhibits a M–NM transition. The effect of disorder on such a model has yet to be explored. A criterion due to Herzfeld (98) states that for a metal, the ratio of molar refractivity and molar volume (R/V) is greater than or equal to unity. This criterion holds for all elemental metals; a thermodynamic criterion based on latent heat of evaporation is found to be equally satisfactory (99).

In the absence of exact models, M–NM transitions in real systems have been explained qualitatively in terms of the available models. For example, for the V_2O_3 transition, Kuwamoto et al (100) proposed a simple model wherein the density of states curve for the *d*-band has a set of high peaks and deep valleys in alternation. The Fermi level in close proximity to one of the minima can be replaced by a band gap that is opened by Cr or Al doping. Change in oxygen stoichiometry or Ti doping shifts the Fermi level so as to render the material metallic. Honig & Spalek (85b) have worked out a thermodynamic model for V_2O_3 that uses different free energy expressions for electrons in the localized and itinerant regimes. Disorder has been invoked to explain transitions in oxide systems such as $La_{1-x}Sr_xVO_3$ (101) and $La_{1-x}Sr_xCoO_3$ (102). Studies of systematics of M–NM transitions across a related series of oxides have yielded valuable results, as discussed in a preceding section. It is noteworthy that in binary

transition metal compounds, the transfer from insulating behavior to metallic behavior occurs in the vicinity of oxides (103).

Before I close this discussion, I briefly present some of the complex oxide systems exhibiting compositionally controlled M–NM transitions that may be especially appealing to chemists. $Ln_{1-x}Sr_xMO_3$ (Ln = La, Pr, Nd; M = V, Mn, Co) show M–NM transitions with increase in x (6a,b, 80). Thus, $La_{1-x}Sr_xCoO_3$ becomes metallic when $x = 0.3$–0.5. Metallicity in the M = Mn and Co systems is accompanied by ferromagnetism. In $LaNi_{1-x}M_xO_3$ (M = Cr, Mn, Fe, or Co), the system goes from having metallic to insulator behavior above a critical value x; at the crossover, the system shows Mott's σ_{min} value. $La_{4-x}Ba_{1+x}Cu_5O_{13+\delta}$ is metallic when $x \approx 0$, but as x increases, it becomes insulating (104). The pyrochlore system $Bi_{2-x}Gd_xRu_2O_7$ exhibits an M–NM transition with increase in x (105).

SUPERCONDUCTIVITY

Although a variety of inorganic and organic solids had been investigated for superconductivity in recent decades, the highest transition temperature attained was around 23K in Nb alloys of the A15 family. Metal oxides had also been explored earlier, and the highest superconducting transition temperature found in them was around 13K in Ba(Pb, Bi)O_3 (9) and $Li_{1+x}Ti_{2-x}O_4$ (19a,b). The new generation of oxide superconductors discovered since the first announcement of 30K superconductivity in $La_{2-x}Ba_xCuO_4$ by Bednorz & Müller (4) has pushed the transition temperature up to 130K. Structure-property relations in the high-temperature superconducting cuprates have been reviewed in some detail very recently (106–110a,b), and references to the original literature on all the aspects discussed here may be found in these and other references cited. I examine here the salient features of these high-temperature superconductors that have caused unprecedented excitement. High T_c superconductivity in cuprates and other oxides has revealed our incomplete knowledge of the electronic structure of transition metal oxide systems.

Properties of Cuprate Superconductors

High-temperature superconducting cuprates discovered in the last two years belong to the following families: (*a*) $La_{2-x}M_xCuO_4$ (M = Ca, Sr, or Ba) of the K_2NiF_4 structure (111–113); (*b*) the $LnBa_2Cu_3O_7$ (123) system (107, 114), where Ln = Y, La, Nd, Sm, Eu, Gd, Dy, Ho, Er, Tm, or Yb; (*c*) the $Bi_2(Ca, Sr)_{n+1}Cu_nO_{2n+4}$ system, with $n = 1, 2, 3, 4$ (110a,b, 115–117); (*d*) the $Tl_2Ca_{n-1}Ba_2Cu_nO_{2n+4}$ system, with $n = 1, 2, 3, 4$ (110a,b, 118–

121); (*e*) the $TlCa_{n-1}Ba_2Cu_nO_{2n+3}$ system, with $n = 1, 2, 3, 4$ (122–124); and (*f*) $Pb_2Sr_2ACu_3O_8$, with A = Ln or Ln+Sr or Ca (125). A three-dimensional oxide without Cu, $Ba_{1-x}K_xBiO_3$ has been found to exhibit (126) a T_c of ~30K. Figure 3 shows the structures of the first three families of cuprates in order to illustrate certain commonalities. The structures of the Tl cuprates are similar to those of the Bi cuprate in Figure 3. All the cuprates, (*a*) to (*f*), possess defect perovskite layers and all but the 123 compounds also contain rock-salt type M–O layers. All of them contain two-dimensional Cu–O sheets, and the 123 compounds have one-dimensional Cu–O chains in addition. The coordination of Cu is essentially square-planar, and the Cu–O bond distance is around 1.9 Å, indicative of high covalency. Oxides of the $La_{2-x}M_xCuO_4$ family are ordinarily tetragonal and become orthorhombic around 180K (127). The T_cs are in the 25–40K range (at an optimal value of x), depending on the M ion. Substitution of La by other rare earth ions or of Cu by Ni, Zn, and similar ions adversely affects the superconducting transition temperature. In the 123 compounds, the Ln ion has little effect on the T_c, but the T_c is markedly dependent on the oxygen stoichiometry, δ. In the case of $YBa_2Cu_3O_{7-\delta}$, T_c is nearly constant (~90K) up to $\delta = 0.2$, but drops to a constant value of ~55K between δ of 0.2 and 0.4; further increase in δ lowers the T_c until it becomes nonsuperconducting when $\delta \approx 0.6$ (128). The structure is orthorhombic over the entire δ range of 0.0–0.60 but becomes tetragonal when $\delta \geq 0.60$. It is not clear whether any special structural feature is associated with the 55K T_c plateau, although the orthorhombic lattice parameters are not related in this region, unlike in the high T_c region ($a \neq b \approx c/3$). Gd and Dy cuprates of this family also show this behavior.

The formal mixed valence of Cu is considered to be essential for the superconductivity in these cuprates. Yet we find superconductivity in $YBa_2Cu_3O_{6.5}$ ($T_c \sim 45$K), which should contain Cu only in the 2+ state. Intergrowth of the O_7 and the O_6 phases is probably responsible for this observation. The presence of Cu^{2+} in $YBa_2Cu_3O_{6.5}$ is evidenced from EPR spectroscopy, in contrast to well-annealed samples with $\delta < 0.2$.

In the 123 compounds, ordered orthorhombic structures with 90K T_c are found only when the 01 oxygen in the Cu–O chains are fully populated and ordered; distribution of the chain oxygen between the 01 and the 05 sites gives rise to disordered orthorhombic structures with low T_cs (129a,b). Equal population of the 01 and 05 sites, just as complete depletion of the 01 oxygen gives rise to tetragonal structures. $YBa_2Cu_3O_{7-\delta}$ samples with high δ can be oxidized to the $\delta \approx 0.0$ composition, but the diffusion of oxygen is a highly activated process.

$LnBa_2Cu_3O_7$ may be considered to be the $x = 1$ member of the more

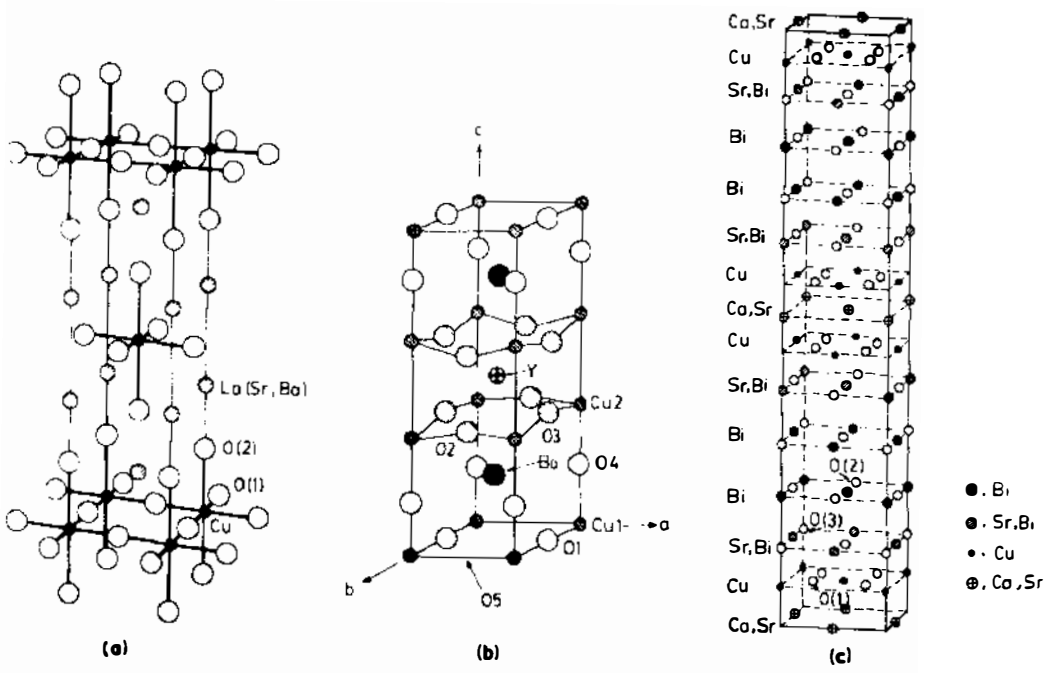

Figure 3 Structures of (*a*) $La_{2-x}M_xCuO_4$ (M = Sr or Ba), (*b*) $YBa_2Cu_3O_7$, and (*c*) $Bi_2(Ca, Sr)_3Cu_2O_8$ (Schematic).

general $Ln_{3-x}Ba_{3+x}Cu_6O_{14+\delta}$ family. A common occurrence in the 336 and 123 compounds is the exchange between the Ln and Ba sites, especially when Ln is a large rare earth ion such as La. Such an exchange does not occur in the $YBa_2Cu_3O_7$ because of the small size of yttrium. The Ba ion in $YBa_2Cu_3O_7$ can be replaced by La, but the T_c is lowered and there is also oxygen excess. The smallest Ln ion tolerated by the 123 structure is Yb.

Orthorhombic 123 compounds show extensive twinning occurring during their formation from the high-temperature tetragonal structures. Across the twin boundaries there is a 90° rotation of the *a* and *b* axes. Although twins may play a crucial role in determining properties such as the critical current density of the 123 compounds, they are not the cause of superconductivity. Thus, orthorhombic $PrBa_2Cu_3O_7$, which is not superconducting, shows twins. The reason for the absence of superconductivity in the 123 compounds of Ce, Pr, and Tb has been suspected to lie in the bivalency (3+ and 4+) of these lanthanide ions, but the exact cause is not yet understood. Orthorhombicity was considered to be a necessary criterion for high T_c in the 123 compounds for some time, but tetragonal $YBa_2Cu_3O_7$, where Co, Fe, or Ga partly substitute for Cu, has since been found to show high T_c behavior; the compounds, however, seem to possess some orthorhombic distortion. Substitution of Cu by Ni and Zn adversely affects the oxygen stoichiometry and lowers the T_c.

Members of the $Bi_2(Ca, Sr)_{n+1}Cu_nO_{2n+4}$ and $Tl_2Ca_{n-1}Ba_2Cu_nO_{2n+4}$ series have similar structures and contain two Bi, Tl–O type rock-salt layers. The bismuth cuprates show modulation in the structure. Members of the $TlCa_{n-1}Ba_2Cu_nO_{2n+3}$ have a single Tl–O type rock-salt layer. The Bi, Ca, and Sr sites in the Bi cuprates are interchangeable, and the compositions are never exactly 2122 or 2223 as described by the general formula. Bi can be partly substituted by Pb (up to ~25%) and this generally favors the formation of better monophasic compositions with slightly enhanced T_cs. In the $Bi_2(Ca, Sr)_{n+1}Cu_nO_{2n+4}$ series, the first three members with *c*-parameters of ~25, 31, and 38 Å have been characterized; the T_cs are 60 ± 20, 85 ± 5, and 107 ± 3K, respectively; the $n = 4$ member also seems to have a T_c close to 110K (117).

In the $Tl_2Ca_{n-1}Ba_2Cu_nO_{2n+4}$ series, the $n = 1$, 2, and 3 members (*c*-parameters 23, 29, and 36 Å) show T_cs of 80, 110, and 125K, respectively. The $n = 2$ and 3 members of the $TlCa_{n-1}Ba_2Cu_nO_{2n+3}$ series show T_cs of 90 and 115K, respectively, which are lower than those of the corresponding members of the Tl_2 series. In the Tl cuprates, just as in the Bi cuprates, we see a progressive increase in T_c as well as in the *c*-parameter with the number of Cu–O sheets only up to $n = 3$ (Figure 4); when $n > 3$, the thallium cuprates do not seem to show a further increase in T_c (121). A

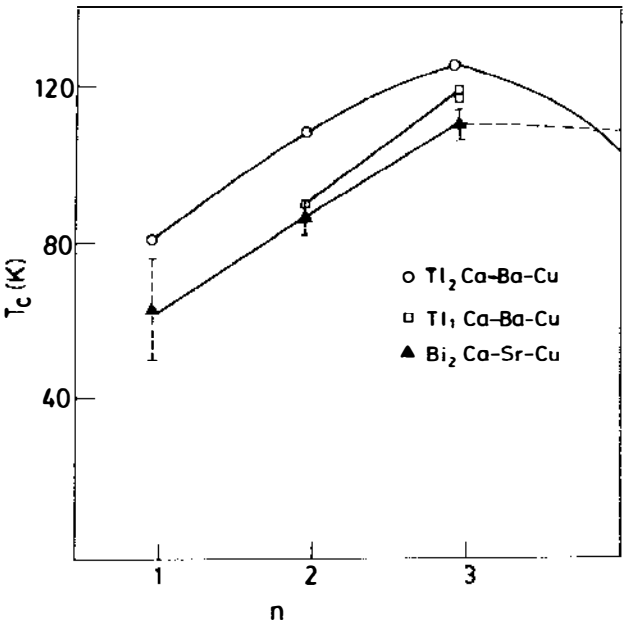

Figure 4 Variation of superconducting transition temperature in thallium and bismuth cuprate systems with the number of Cu–O sheets.

feature common to the Bi and Tl cuprates is the presence of disordered intergrowths (58). It is noteworthy that $YBa_2Cu_4O_8$ with two Cu–O chains (edge-shared square planar units) has only a T_c of ~80K compared to ~90K of $YBa_2Cu_3O_7$ (130).

It has not been possible to prepare well-defined superconducting compositions of the Tl–Ca–Sr–Cu–O system with the general formula $Tl_{1,2}(Ca, Sr)_{n+1}Cu_nO_{2n+3,4}$. These members are, however, stabilized by partial substitution of Tl by Pb (131a,b). Thus, progressive increase in x in $Tl_{1-x}Pb_xCaSr_2Cu_2O_y$ increases the T_c up to 90K when $x = 0.5$; $Tl_{0.5}Pb_{0.5}CaSr_2Cu_3O_7$ has a T_c of 120K. Progressive substitution of Ca by Y in $TlCa_{n-1}Ba_2Cu_nO_{2n+3}$ and $Bi_2(Ca, Sr)_{n+1}Cu_nO_{2n+4}$ lowers the T_c, until superconductivity is lost upon complete replacement (132a). The layered Pb cuprates (125) contain Cu mainly in the 1+ state (132b) and show T_c around 70K. Whereas Pb in $Pb_2Sr_2Ca_{1-x}\ln_x Cu_3O_8$ is mainly in the 2+ state, in $Tl_{0.5}Pb_{0.5}CaSr_2Cu_3O_7$ and $Bi_{1+5}Pb_{0.5}(Ca, Sr)_{n+1}Cu_nO_{2n+4}$ it is in the 4+ state (C. N. R. Rao, unpublished results). Recently, a series of cuprates of the formula $TlCa_{1-x}\ln_x Sr_2Cu_2O_{7+\delta}$ with T_c in the 60–90K range has been discovered (132c). There is a possibility of competition between electron and hole superconductivity in this system.

Properties of Superconducting Cuprates

Some of the relevant properties of the superconducting state are the critical field, the critical current, the magnetic penetration depth, and the coherence length. The $H_{c1}(O)$ and $H_{c2}(O)$ of $YBa_2Cu_3O_7$ parallel to the *c*-axis are around 1 and 120T, respectively; the magnetic penetration depth is $\sim$900 Å. The coherence length (size of the Coopcr pair) is 10–30 Å in the *ab*-plane of $YBa_2Cu_3O_7$ as well as other cuprates, but only about 3 Å perpendicular to the plane (133). The meaning of such a small coherence length is not clear. Anisotropy is also found in the magnetic and electrical propcrties of $YBa_2Cu_3O_7$ and the other cuprates. The critical current of a superconductor should be at least $\sim 10^5$ amp cm^{-2} for magnetic and other applications at the operating temperatures. Although values of 10^5 amps cm^{-2} or higher have been reported in films and single grain materials of $YBa_2Cu_3O_7$, it has not been possible to obtain good, reproducible samples because of the presence of grain boundaries and weak flux pinning. The situation is the same with Ti and Bi cuprates.

No measurable ^{18}O isotope effect has been observed in $YBa_2Cu_3O_7$ (134). Infrared absorption, point-contact tunnelling spectroscopy, and other measurements (135) suggest the superconducting gap, 2Δ, to be around 3–4 (k_BT_c). It is not yet clear whether there is a specific heat discontinuity at T_c in the oxide superconductors.

The Cu ions in the superconducting cuprates are EPR-silent, but the cuprates show intense nonresonant absorption of microwaves (136a,b). The presence of Cu^{2+} in $YBa_2Cu_3O_{7-\delta}$ is seen from magnetic measurements in the non-superconducting $YBa_2Cu_3O_6$, which is antiferromagnetic (T_N = 450K). $LnBa_2Cu_3O_7$ compounds with Ln = Gd, Dy, etc show magnetism at low temperatures due to the Ln ion (137).

The *d–d* correlation energy is the largest relevant energy in these oxides. The density of states near the Fermi energy in La_2CuO_4 and $La_{2-x}M_xCuO_4$ is small as revealed by photoemission spectra. An angle-resolved photoemission study of $Bi_2CaSr_2Cu_2O_8$ has shown that there are *p*-like bands near and below E_F, with a very small width ($\sim$0.5 eV). It appears that $(\varepsilon_p - \varepsilon_d)$ is around 1–3 eV, and the *pd* mixing integral t_0 is in the range of 1–2 eV (138).

Nature of Copper and Oxygen

The state of copper in the cuprate superconductors is of seminal importance to the mechanism of superconductivity in these materials. In stoichiometric La_2CuO_4, Cu is present in the 2+ state; this would not be the case in $La_{2-x}M_xCuO_4$ or $YBa_2Cu_3O_7$. It has been generally believed that the presence of Cu in the mixed valent (2+, 3+) state, in such doped

oxides, is essential to explain the magnetic and superconducting properties. Oxygen-excess in these materials is expected to create holes on Cu in the form of Cu^{3+}. However, X-ray absorption and photoemission measurements show no evidence for the presence of Cu^{3+} in $YBa_2Cu_3O_7$. Instead, they show the presence of copper in the 1+ state and holes on oxygen, O^{1-} (139–141). This is corroborated by electron energy loss spectroscopy, which shows an *s–p* transition of oxygen (142). X-ray photoelectron spectroscopy and Auger spectroscopy also show that for all practical purposes, there is no Cu^{3+} in $YBa_2Cu_3O_7$, $Bi_2(Ca, Sr)_3Cu_2O_{8+\delta}$, and $Tl_2CaBa_2Cu_2O_8$, but there is evidence for the presence of the Cu^{1+} state. Evidence for the dimerization of oxygen holes giving rise to peroxo-type species, O_2^{2-}, has also been presented based on O(1*s*) spectra. It is believed by many workers today that mobile oxygen holes are responsible for the superconductivity of the cuprates. In the Bi and Tl cuprates, the Bi–O and Tl–O layers seem to donate such holes.

Chakraverty et al (143) have proposed that the $d_{x^2-y^2}$ orbital of copper (in the Cu–O sheets) overlaps with the p_σ orbital of oxygen (formed by a combination of p_x and p_y orbitals), forming a broad Cu–O band consistent with high covalency of the Cu–O bands. They also propose that the holes are in the p_σ state (within the Cu–O band) and that they are more favored by the d^{10} state Cu^{1+} ions than by $Cu^{2+}(d^9)$ ions. They suggest that a O^{1-}–Cu^{+}–O^{1-} state (designated as a peroxiton) is energetically favored compared to a hole bipolaron, O^{1-}–Cu^{2+}–O^{1-}. The presence of holes in p_σ also explains the absence of anti-ferromagnetism in the cuprates. Guo, Langlois & Goddard (144) suggest, based on cluster calculations, that oxidation of Cu beyond Cu^{2+} creates oxygen p_Π holes bridging two Cu^{2+} sites. The p_Π holes are ferromagnetically coupled to adjacent Cu^{2+} *d*-electrons, and hopping of the p_Π holes in the Cu–O sheets from sitc to site is responsible for the conductivity. The p_Π of these workers is not the p_z orbital but a $p_{x,y}$ orbital of oxygen. It is not clear that these will form narrow bands distinctly separated from the broad Cu–O band involving $d_{x^2-y^2}$ (Cu) and oxygen p_σ orbitals. High energy spectroscopy experiments (145a,b) clearly show that the holes are in the CuO_2 planes and have essentially $p_{x,y}$ character. Cluster calculations support existence of the copper states found from core level spectroscopies (146). Oxygen hole-pairing has been suggested by a few theoreticians (147, 148). We can relate the presence of O^{1-} holes to the average charge, *p*, of $(Cu–O)^p$, since *p* is known to be related to the superconducting properties of the cuprates (149a). A finite positive value of *p* can only result from $(Cu^{2+}–O^{1-})^{1+}$ in combination with $(Cu^{2+}–O^{2-})^0$ and $(Cu^{1+}–O^{1-})^0$ and the relative importance of the last two may determine whether a particular cuprate is a superconductor or an insulator. The importance of oxygen holes is also

underscored by the discovery of relatively high T_c in $Ba_{1-x}K_xBiO_3$ (126). In the Pb cuprates (125), there is no possibility of Cu^{3+} occurring, even according to the chemical formula, and this would suggest a role for Cu^{1+} (132b), proposed earlier for 123 oxides and other systems (140a–c). The discovery of the so-called electron superconductor $Nd_{2-x}Ce_xCuO_4$ (149b) is interesting, but it is not yet clear that the electron donated by Ce goes to the Cu 3*d* orbital (149c).

Theoretical Approaches

Models for the electronic structures of superconducting cuprates range from the strong crystal field limit to the correlated weak crystal field limit. A one-band Hubbard model with a novel ground state involving low-spin Cu has been proposed (150). A simple two-band model with a strongly correlated *d*-type band and weakly correlated *p*-type band hybridizing with it has been examined (147, 151). There are, however, many real complications with these models (152). Electronic structure calculations are believed to be inadequate in highly correlated systems. Useful information has been obtained, however, from self-consistent one-electron theory as well as from numerical calculations on Cu–O clusters (153, 154). Calculations on the problem of two holes hybridizing with the oxygen *p*-band have also been performed (155).

Any theoretical model has not only to explain the varied properties of the superconducting state, such as the short coherence length, non-exponential dependence of NMR relaxation rate on temperature, the energy gap, resistivity and heat capacity behavior near T_c, etc, but also the optical, magnetic, transport, NMR relaxation, and other properties of the normal state (152). A number of models have been proposed. They make use of both phonon and electronic mechanisms. A spin-bag theory has been discussed (156). The most original idea is the resonating valence band theory of Anderson and co-workers (150, 157). In this theory, the spin 1/2 of the d^9 configuration and two dimensionality of the Cu–O layers make for a non-Neèl magnetic ground state (the RVB state) with characteristic excitations. Singlet pairs present in this ground state are preformed Cooper pairs with a binding energy close to *J* and of the size of interatomic spacing. Upon introduction of holes, this system transports charge and becomes a superconductor. Hole-pairing via interlayer hopping has also been considered (158). Correlated electron models have been used to examine the problem of hole mobility or the attraction of charge carriers (152). The nature of oxygen defects and the Fermi level location in $YBa_2Cu_3O_{7-\delta}$ and $La_2CuO_{4-\delta}$ have been examined in the light of tight-binding calculations (159).

SYNTHESIS AND CHARACTERIZATION

A wide range of conditions have been employed to synthesize transition metal oxides. These include high temperatures and pressures, carefully controlled oxidizing or reducing atmospheres, hydrothermal conditions, skull and arc melting, and so on (3, 160, 161). Oxides are most commonly prepared by the ceramic method, involving repeated grinding and heating of the reactant powders of oxides, carbonates, etc (often in pellet form) or sealed tube reactions. There has been increasing interest in preparing oxides under milder, less energy-consuming conditions. The precursor method has been employed effectively to achieve homogeneous mixing of reactant species on an atomic scale (162). This method reduces the diffusion distances to 100 Å or so instead of 10,000 Å or more in the ceramic method. Besides precursor compounds, solid solutions of carbonates, nitrates, hydroxides, and cyanides have been employed for the purpose. The method also enables the synthesis of novel oxides, which are otherwise difficult to prepare. Topochemical reactions similarly yield unusual oxides; e.g. the synthesis of MoO_3 of ReO_3 structure by the topochemical dehydration of $MoO_3 \cdot H_2O$ is a good example (163a,b). $Mo_{1-x}W_xO_3$ has also been prepared by such a dehydration reaction. Many examples of topochemical reactions giving novel oxides are reported in the literature (3, 162). A topochemical reaction deserving special mention is the insertion of atomic species into oxide hosts (164). Thus, lithium and other alkali metals have been inserted into a variety of oxides such as VO_2, TiO_2, MnO_2, ReO_3, and Fe_3O_4. The subject of intercalation has been reviewed adequately in the literature (3, 164, 165). Deintercalation of lithium and other species can be carried out readily by employing mild oxidizing conditions. Many new examples of intercalation and deintercalation are constantly being reported. Recently, topochemical reactions of Li_xNbO_2 (166) and lithium insertion to $W_{19}O_{55}$ (167) have been reported.

Ion exchange has been carried out in oxides having layered, tunnel, or close-packed structures. Such reactions are also topochemical and are carried in aqueous solutions or molten media (3, 162). Conversion of $LiNbO_3$ to $HNbO_3$ by treatment with hot aqueous acid is an example (168). The mechanism of this reaction appears to be reverse of the transformation of ReO_3 to rhombohedral $LiReO_3$ (169). Hydrogen can also be inserted into oxide holes in the presence of a Pt catalyst (162). Potentialities of exchange reactions for synthetic purposes are immense. Many interesting exchange reactions have been reported in the literature; two recent examples are the effect of intercalated alkylammonium ion on the cation exchange properties of $H_2Ti_3O_7$ and the exchange properties of

$Na_4Ti_9O_{20} \cdot x \cdot H_2O$ (170a,b). Synthesis of metastable TiO_2 and layered $K_2Ti_4O_9$ by a topotactic dehydroxylation is another interesting example (171).

Among the other chemical methods of synthesis, the chemical vapor deposition technique is well known. Fused salt electrolysis has been employed to synthesise oxides such as complex oxides of Mo and Mo bronzes (28, 172a,b). The pyrochlores $Pb_2[Ru_{2-x}Pb_x^{4+}]O_{7-y}$ and $Bi[Ru_{2-x}Bi_x^{5+}]O_{7-y}$ have been prepared from a strongly alkaline medium under oxidizing conditions (173). The sol-gel route has proved to be extremely successful in synthesizing a variety of oxides (3, 162, 174), including the superconducting cuprates (175).

Many oxides have been prepared by arc melting. A novel method of preparing some of the transition metal oxides is by the crucible-free method (176). Single crystals of complex oxides such as La_2NiO_4 and Fe_3O_4 have been prepared by such skull melting. High pressure methods in synthesis have been reviewed (3, 177, 178). Use of high pressure enables stabilization of unusual oxidation states (e.g. $CaCrO_3$, $La_2Pd_2O_7$, $GdNiO_3$). Fe(V) has been stabilized in La_2LiFeO_6; high-spin Fe(IV), low-spin Ni(III), and Co(IV) are the other states so stabilized under high oxygen pressure. $YBa_2Cu_4O_8$ has been prepared recently under high oxygen pressure (130).

Techniques of characterization of oxide materials have advanced rapidly in the last decade (3, 179). Although single crystal X-ray crystallography continues to be a useful technique, profile analysis of X-ray and neutron diffraction patterns of powders by the Rietveld method has emerged to become a powerful tool (179, 180). A new generation of ultra-high resolution powder X-ray and neutron diffractometers (181, 182) allows *ab initio* determination of oxide structures by using synchrotron X-rays and high-intensity (spallation) neutron sources (183, 184). Epithermal neutrons are useful to study crystal field transitions in oxides such as PrO_2 and $BaPrO_3$ (185).

High-resolution electron microscopy has been used routinely to study local structure of oxides at atomic and unit cell levels. Composition characterization by X-ray emission, electron energy loss spectroscopy, etc carried out in the electron microscope is becoming more useful for heavy elements and also for oxygen (186a–c). Electron energy loss spectroscopy is also useful in characterizing oxidation states of metals (187), and the technique has been reviewed recently (188).

High-resolution NMR spectroscopy has been of great value in the study of zeolites and other oxidic materials. The technique has also been useful in the study of phase transitions and other phenomena, but a wider use employing transition metal nuclei is likely in the future. EXAFS, XANES, and related X-ray absorption techniques are useful in determining the

oxidation state and coordination of the transition metal ion in complex oxide materials (including catalysts), as illustrated by the recent studies on cuprate superconductors (139–141). Electron spectroscopies (XPS, UPS, Auger, EELS, etc) have been used widely to investigate transition metal oxides; a noteworthy technique to study electron states of the metal is the one based on Auger intensity ratios (189a–c). These high-energy spectroscopies have played an important role in determining the states of copper and oxygen in superconducting cuprates (140–141). Scanning tunneling microscopy (190a,b) is now another powerful tool in the arsenal of solid state scientists to study oxide materials.

EPILOGUE

We are yet a long way from fully understanding the electronic structures and properties of transition metal oxides. Considerable scope remains for carrying out good measurements, designing novel oxides with desired properties, and developing useful models. High T_c superconducting oxides are all quasi two-dimensional cuprates. There is a good probability that high T_c will be discovered in other oxide materials, including three-dimensional systems. In this context, the possible occurrence (12c,d) of superconductivity in layered nickelates is noteworthy. It is also interesting that the 30K superconductor $Bi_{1-x}K_xBiO_3$ has rather unusual properties, such as a large ^{18}O isotope effect (191) and the absence of static magnetic order (192), unlike in the cuprates. An important aspect that needs to be understood is the role of holes on oxygen (O^{1-}) and their possible dimerization (O_2^{2-}) in transition metal oxides. Holes on oxygen have been found in many transition metal oxides purported to contain the metals in high oxidation states, such as $La_2NiO_{4+\delta}$, $LiNiO_2$, $LaNiO_3$, and $Ba_2Cu_2O_5$ (143, 193, 194; C. N. R. Rao et al, unpublished results). It is known that anion hole pairing gives rise to S–S, Se–Se, and Te–Te bonds in the chalcogenides containing $Cu^{1+}(d^{10})$ ions. There is some evidence that peroxide-like species arising from hole pairing may be present in certain transition metal oxides, including the superconducting cuprates (195). Unless the exact description of the states of oxygen and the metal ions becomes possible, understanding the properties of transition metal oxides will be difficult. In this regard, a breakthrough is needed in theoretical approaches to understand phenomena such as metal-insulator transitions and superconductivity in transition metal oxides.

ACKNOWLEDGMENTS

I thank the Department of Science and Technology, the University Grants Commission, and the US National Science Foundation for supporting my research efforts in transition metal oxides.

Literature Cited

1. Rao, C. N. R., Subbarao, G. V. 1970. *Phys. Status Solidi A* 1: 597–652; Rao, C. N. R., Subbarao, G. V. 1974. *Transition Metal Oxides*, NSRDS-NBS Monogr. 49. Washington, DC: Natl. Bur. Stand.
2. Goodenough, J. B. 1971. *Progr. Solid State Chem.* 5: 149–399; Goodenough, J. B. 1974. In *Solid State Chemistry*, ed. C. N. R. Rao. New York: Dekker; Goodenough, J. B. 1963. *Magnetism and the Chemical Bond*. New York: Wiley
3. Rao, C. N. R., Gopalakrishnan, J. 1986. *New Directions in Solid State Chemistry*. Cambridge: Cambridge Univ. Press
4. Bednorz, J. G., Müller, K. A. 1986. *Z. Phys. B* 64: 189–96
5. Vasanthacharya, N. Y., Ganguly, P., Goodenough, J. B., Rao, C. N. R. 1984. *J. Phys. C* 17: 2745–60

6a. Rao, C. N. R., Ganguly, P. 1985. In *Localization and Metal–Insulator Transitions*, ed. D. Adler, H. Fritzsche. New York: Plenum

6b. Rao, C. N. R., Prakash, O., Bahadur, D., Ganguly, P., Nagabhushana, S. 1977. *J. Solid State Chem.* 22: 353–64

7. Goodenough, J. B., Longo, J. M. 1970. *Landolt-Börnstein Tabellen*, New Ser., III/4a. Berlin: Springer-Verlag
8. Nomura, S. 1978. *Landolt-Börnstein Tabellen*, New Ser., III/12a. Berlin: Springer-Verlag
9. Sleight, A. W., Gillson, J. L., Bierstedt, F. E. 1975. *Solid State Commun.* 17: 27–31
10. Ganguly, P., Rao, C. N. R. 1984. *J. Solid State Chem.* 53: 193–216
11. Mohan Ram, R. A., Ganguly, P., Rao, C. N. R., Honig, J. M. 1988. *Mater. Res. Bull.* 23: 501–5

12a. Shirane, G., Endoh, Y., Birgneau, R. J., Katsner, M. A., Hidaka, Y., Oda, M., Suzuki, M., Murakami, T. 1987. *Phys. Rev. Lett.* 59: 1613–15

12b. Aeppli, G., Buttrey, D. J. 1988. *Phys. Rev. Lett.* 61: 203–5

12c. Rao, C. N. R., Ganguli, A. K., Nagarajan, R. 1989. *Pramana J. Phys.* 32: 177–80

12d. Spalek, J., Kakol, Z., Honig, J. M. 1989. *Phys. Rev. Lett.* To be published

13a. Mohan Ram, R. A., Ganapathi, L., Ganguly, P., Rao, C. N. R. 1986. *J. Solid State Chem.* 63: 139–47

13b. Rao, C. N. R., Ganguly, P., Singh, K. K., Mohan Ram, R. A. 1988. *J. Solid State Chem.* 72: 14–23

14a. Aurivillius, B. 1950. *Akiv Kemi* 2: 519–27

14b. Hutchison, J. L., Anderson, J. S., Rao, C. N. R. 1977. *Proc. R. Soc. London Ser. A* 355: 301–13

15. Portier, R., Carpy, A., Fayard, M., Galy, J. 1975. *Phys. Status Solidi A* 30: 683–89
16. Englman, R. 1972. *The Jahn-Teller Effect in Molecules and Crystals*. London: Wiley
17. Gehring, G. A., Gehring, K. A. 1975. *Rep. Prog. Phys.* 38: 1–89
18. Rao, C. N. R., Rao, K. J. 1978. *Phase Transitions in Solids*. New York: McGraw-Hill

19a. Johnston, D. C., Prakash, H., Zachariasen, W. H., Viswanathan, R. 1973. *Mater. Res. Bull.* 8: 777–82

19b. Lambert, P. M., Harrison, M. R., Edwards, P. P. 1988. *J. Solid State Chem.* 75: 332–46

20. Muraleedharan, K., Srivastava, J. K., Marathe, V. R., Vijayaraghavan, R., Kulkarni, J. A., Darshane, V. S. 1985. *Solid State Commun.* 55: 363–66
21. Subramanian, M. A., Aravamudan, G., Subbarao, G. V. 1983. *Progr. Solid State Chem.* 15: 55–143
22. Subramanian, M. A., Torardi, C. C., Johnson, D. C., Pannetier, J., Sleight, A. W. 1988. *J. Solid State Chem.* 72: 24–30
23. Beyerlein, R. A., Horowitz, H. S., Longo, J. M. 1988. *J. Solid State Chem.* 72: 2–13
24. Rao, C. N. R. 1985. *Int. Rev. Phys. Chem.* 4: 19–38
25. Imoto, H., Simon, A. 1982. *Inorg. Chem.* 21: 308–14

26a. Kihlborg, L. 1978. *Chem. Scr.* 14: 187–97

26b. Eckstrom, T., Tilley, R. J. D. 1980. *Chem. Scr.* 16: 1–16

26c. Ramanan, A., Gopalakrishnan, J., Uppal, M. K., Jefferson, D. A., Rao, C. N. R. 1984. *Proc. R. Soc. London Ser. A* 395: 127–40

27a. Hagenmuller., P. 1971. *Progr. Solid State Chem.* 5: 71–144

27b. Doumerc, J. P., Pouchard, M., Hagenmuller, P. 1985. See Ref. 84, pp. 287–328

28. Greenblatt, M. 1988. *Chem. Rev.* 88: 31–53

29a. Collins, B. T., Ramanujachary, K. V., Greenblatt, M., McCarroll, W. H., McNally, P., Waszczak, J. V. 1988. *J. Solid State Chem.* 76: 319–27

29b. Tsai, P. P., Potenza, J. A., Greenblatt,

M. 1987. *J. Solid State Chem.* 69: 329–35
30. Barbara, T. M., Gammie, G., Lyding, J. W., Jonas, J. 1988. *J. Solid State Chem.* 75: 183–87
31a. Domenges, B., Goreand, M., Labbe, Ph., Raveau, B. 1983. *J. Solid State Chem.* 50: 173–80
31b. Hervieu, B., Domenges, B., Raveau, B. 1985. *Chem. Scr.* 54: 10–16
31c. Domenges, B., Hervieu, M., Raveau, B., O'Keefee, M. 1988. *J. Solid State Chem.* 72: 155–72
32. Wang, E., Greenblatt, M. 1988. *J. Solid State Chem.* 76: 340–44
33. Ganguli, A. K., Ganapathi, L., Gopalakrishnan, J., Rao, C. N. R. 1988. *J. Solid State Chem.* 74: 228–31
34. Newnham, R. E., Cross, L. E. 1981. In *Preparation and Characterization of Materials*, ed. J. M. Honig, C. N. R. Rao. New York: Academic
35. Anderson, J. S., Tilley, R. J. D. 1974. In *Surface and Defect Properties of Solids*, ed. M. W. Roberts, J. M. Thomas, Vol. 3. London: Chem. Soc.
36. Anderson, J. S. 1984. *Proc. Indian Acad. Sci.* (*Chem. Sci.*) 93: 861–904
37. Watanabe, D., Tearesaki, O., Jostons, A., Castles, J. R. 1970. In *The Chemistry of Extended Defects in Nonmetallic Solids*, ed. L. Eyning, M. O'Keeffe. Amsterdam: North-Holland
38. Terauchi, H., Cohen, J. B. 1979. *Acta Cryst. A* 35: 646–52
39. Morinaga, M., Cohen, J. B. 1979. *Acta Cryst. A* 35: 745–54, 975–80
40. Gavarri, J. 1978. Doctoral thesis. Univ. Paris VI
41. Catlow, C. R. A., Mackrodt, W. C., eds. 1982. *Computer Simulation of Solids. Lect. Notes Phys.* Berlin: Springer-Verlag
42. Bauer, E., Pianelli, A., Aubry, A., Jeannot, F. 1980. *Mater. Res. Bull.* 15: 323–28
43. Garstein, E., Mason, T. O., Cohen, J. B. 1986. *J. Phys. Chem. Solids* 47: 759–73
44. Tetot, R., Gerdanian, P. 1985. *J. Phys. Chem. Solids* 46: 1131–39
45. Grimes, R. W., Anderson, A. B., Heuer, A. H. 1986. *J. Am. Ceram. Soc.* 69: 619–23
46. Men, A. N., Carel, C. 1985. *J. Phys. Chem. Solids* 46: 1185–93
47. Thornber, M. R., Bevan, D. J. M. 1970. *J. Solid State Chem.* 1: 536–42
48. Catlow, C. R. A., Chadwick, A. V., Corish, J. 1983. *J. Solid State Chem.* 48: 65–72
49. Tilley, R. J. D. 1980. In *Chemical Physics of Solids and Surfaces*, ed. M. W. Roberts, J. M. Thomas, Vol. 8. London: Chem. Soc.
50. Catlow, C. R. A., James, R. 1980. In *Chemical Physics of Solids and Surfaces*, ed. M. W. Roberts, J. M. Thomas, Vol. 8. London: Chem. Soc.
51. Blanchin, M. G., Bursill, L. A., Smith, D. J. 1984. *Proc. R. Soc. London Ser. A* 391: 351–63; Bursill, L. A., Blanchin, M. G., Smith, D. J. 1984. *Proc. R. Soc. London Ser. A* 391: 373–85
52. Bursill, L. A., Smith, D. J. 1984. *Nature* 309: 319–21
53. Millot, F., Blanchin, M. G., Tetot, R., Marucco, J. F., Poumellec, B., Picard, C., Touzelin, B. 1987. *Prog. Solid State Chem.* 17: 263–93
54. Wadsley, A. D., Andersson, S. 1970. In *Perspectives in Structural Chemistry*, ed. J. D. Dunitz, J. A. Ibers, Vol. 3. New York: Wiley
55. Gruehn, R., Mertin, M. 1980. *Angew. Chem. Int. Ed. Engl.* 19: 505–12
56. Anderson, J. S. 1973. *J. Chem. Soc. Dalton Trans.* 1973: 1107–15
57. Kittel, C. 1978. *Solid State Commun.* 25: 319–22
58a. Rao, C. N. R., Thomas, J. M. 1985. *Acc. Chem. Res.* 18: 113–18
58b. Rao, C. N. R. 1985. *Bull. Mater. Sci.* 7: 155–70
59. Vidyasagar, K., Ganapathi, L., Gopalakrishnan, J., Rao, C. N. R. 1986. *J. Chem. Soc. Chem. Commun.*, pp. 449–50
60. Battle, P. D., Gibb, T. C., Lightfoot, P. 1988. *J. Solid State Chem.* 76: 334–39
61a. Alario-Franco, M. A., Gonzalez, J. M. G., Valletregi, M., Grenier, J. C. 1983. *J. Solid State Chem.* 49: 219–27
61b. Gonzalez, J. M. G., Valletregi, M., Alario-Franco, M. A., Grenier, J. C. 1983. *Mater. Res. Bull.* 18: 285–90
62. Rodriguez, J., Fontcuberta, J., Longworth, G., Valletregi, M., Gonzalez, J. M. G. 1988. *J. Solid State Chem.* 73: 57–64
63. Caignaert, V., Hervieu, M., Domenges, B., Nguyen, N., Pannetier, J., Raveau, B. 1988. *J. Solid State Chem.* 73: 107–17
64. Reller, A., Thomas, J. M., Jefferson, D. A., Uppal, M. K. 1984. *Proc. R. Soc. London Ser. A* 394: 223–35
65. Takano, M., Okita, T., Nakayama, N., Bando, Y., Takeda, Y., Yamamoto, O., Goodenough, J. B. 1988. *J. Solid State Chem.* 73: 140–48
66. Rao, C. N. R., Gopalakrishnan, J., Vidyasagar, K. 1984. *Indian J. Chem. A* 23: 265–78
67. Burdett, J. K., Kulkarni, G. V. 1988. *J. Am. Chem. Soc.* 110: 5361–68

68. Ehlert, M. K., Greedan, J. E., Subramanian, M. A. 1988. *J. Solid State Chem.* 75: 188–96
69. Poeppelmeier, K. R., Leonowicz, M. E., Scanlon, J. C., Longo, J. M., Yelon, W. B. 1982. *J. Solid State Chem.* 45: 71–77
70. Vidyasagar, K., Gopalakrishnan, J., Rao, C. N. R. 1985. *Inorg. Chem.* 23: 1206–11
71. Buttrey, D. J., Ganguly, P., Honig, J. M., Rao, C. N. R., Schartman, R. R., Subbanna, G. N. 1988. *J. Solid State Chem.* 74: 233–37
72. Day, P. 1981. *Int. Rev. Phys. Chem.* 1: 149–94
73. Varma, C. M. 1985. *Comments Solid State Phys.* 11: 221–24
74. Subbarao, G. V., Ramdas, S., Mehrotra, P. N., Rao, C. N. R. 1970. *J. Solid State Chem.* 2: 377–84
75. Ganguly, P., Hegde, M. S. 1988. *Phys. Rev. B* 37: 1988–92
76a. Aragon, R., Buttrey, D. J., Shepherd, J. P., Honig, J. M. 1985. *Phys. Rev. B* 31: 430–38
76b. Honig, J. M. 1986. *Proc. Indian Acad. Sci. Chem. Sci.* 96: 391–410
77. Honig, J. M. 1985. See Ref. 84, pp. 261–86
78. Bhide, V. G., Rajoria, D. S., Rao, C. N. R., Ramarao, G., Jadhao, V. G. 1975. *Phys. Rev. B* 12: 2832–44
79. Ramdani, A., Gleitzer, C., Gavoille, G., Cheetham, A. K., Goodenough, J. B. 1985. *J. Solid State Chem.* 60: 269–82
80. Rao, C. N. R., Ganguly, P. 1985. See Ref. 84, pp. 329–58
81. Gibb, T. C., Greatrex, R., Greenwood, N. N., Puxley, D. C., Snowdon, K. G. 1974. *J. Solid State Chem.* 11: 17–25
82. Rao, C. N. R. 1987. In *Valence Fluctuation*. New York: Plenum
83. Mott, N. F. 1974. *Metal-Insulator Transitions*. London: Taylor & Francis; Mott, N. F. 1984. *Rep. Prog. Phys.* 47: 909–23
84. Edwards, P. P., Rao, C. N. R., eds. 1985. *The Metallic and the Nonmetallic States of Matter*. London: Taylor & Francis
85a. Honig, J. M., Van Zandt, L. L. 1975. *Annu. Rev. Mater. Sci.* 5: 225–50
85b. Honig, J. M., Spalek, J. 1986. *Proc. Indian Natl. Sci. Acad. A* 52: 232–64
86. Milligan, R. F., Thomas, G. A. 1985. *Annu. Rev. Phys. Phys. Chem.* 36: 139–58
87. Villeneuve, G., Hagenmuller, P. 1985. In *Localization and Metal-Insulator Transitions*, ed. H. Fritzsche, D. Adler. New York: Plenum
88. Ramakrishnan, T. V. 1985. See Ref. 84, pp. 23–64; Ramakrishnan, T. V. 1985. *Proc. Indian Natl. Sci. Acad. A* 52: 217–31
89. Hubbard, J. 1964. *Proc. R. Soc. London Ser. A* 281: 401–15
90. Economu, E. N. 1981. *Phys. Rev. B* 24: 5806–14
91. Gutzwiller, M. C. 1965. *Phys. Rev. A* 137: 1726–33
92. Brinkman, W., Rice, T. M. 1970. *Phys. Rev. B* 2: 4302–6
93. Anderson, P. W. 1958. *Phys. Rev.* 109: 1492–1504
94. Mott, N. F., Davis, E. A. 1979. *Electronic Processes in Noncrystalline Solids*. Oxford: Clarendon. 2nd ed.
95. Abrahams, E. A., Anderson, P. W., Licciardello, D. C., Ramakrishnan, T. V. 1979. *Phys. Rev. Lett.* 42: 673–76
96. Lee, P. A., Ramakrishnan, T. V. 1985. *Rev. Mod. Phys.* 57: 287–337
97. Edwards, P. P., Sienko, M. J. 1981. *J. Am. Chem. Soc.* 103: 2967–72
98. Herzfeld, K. F. 1927. *Phys. Rev.* 29: 701 5
99. Rao, C. N. R., Ganguly, P. 1986. *Solid State Commun.* 57: 5–6
100. Kuwamoto, H., Honig, J. M., Appel, J. 1980. *Phys. Rev. B* 22: 2626–32
101. Mott, N. F., Pepper, M., Pollitt, S., Wallis, R. H., Adkins, C. J. 1975. *Proc. R. Soc. London Ser. A* 345: 169–80
102. Rao, C. N. R., Bhide, V. G., Mott, N. F. 1975. *Philos. Mag.* 32: 1277–81
103. Wilson, J. A. 1985. See Ref. 84, pp. 215–60
104. Vijayaraghavan, R., Mohan Ram, R. A., Ganguly, P., Rao, C. N. R. 1988. *Mater. Res. Bull.* 23: 719–23
105. Goodenough, J. B., Hamnett, A., Teller, D. 1985. In *Localization and Metal-Insulator Transitions*, ed. H. Fritzsche, D. Adler. New York: Plenum
106. Nelson, D. L., Whittingham, M. S., George, T. F., eds. 1987. *Chemistry of High-Temperature Superconductors*, ACS Symp. Ser. 351. Washington, DC: Am. Chem. Soc.
107. Rao, C. N. R. 1988. *J. Solid State Chem.* 74: 147–62; Rao, C. N. R. 1988. *Mod. Phys. Lett. B* 2: 1217–21
108. Rao, C. N. R., ed. 1988. *Chemistry of Oxide Superconductors*. Oxford: IUPAC/Blackwell
109. Müller, J., Olsen, J. L., eds. 1988. *Proc. Interlaken M^2HTSC Conf. Physica C* 153–155: 1–1774
110a. Rao, C. N. R., ed. 1988. *Chemical and Structural Aspects of High-Temperature Superconductors, Progress in High-*

Temperature Superconductivity, Vol. 7. Singapore: World Scientific
110b. Rao, C. N. R., Raveau, B. 1989. *Acc. Chem. Res.* 22: 106–13
111. Uchida, S., Takagi, H., Kitazawa, K., Tanaka, S. 1987. *Jpn. J. Appl. Phys.* 26: L1–4
112. Chu, C. W., Hor, P. H., Meng, R. L., Gao, L., Huang, Z. J., Wang, Y. Q. 1987. *Phys. Rev. Lett.* 58: 405–9
113. Ganguly, P., Mohan Ram, R. A., Sreedhar, K., Rao, C. N. R. 1987. *Solid State Commun.* 62: 807–10
114. Wu, M. K., Ashburn, J. R., Torng, C. J., Hor, P. H., Meng, R. L. et al. 1987. *Phys. Rev. Lett.* 58: 908–11
115. Maeda, H., Tanaka, Y., Fukutomi, M., Asano, T. 1987. *Jpn. J. Appl. Phys.* 27: L209–13
116. Subramanian, M. A., Torardi, C. C., Calabrese, J. C., Gopalakrishnan, J., Morrissey, K. J., et al. 1988. *Science* 239: 1015–17
117. Rao, C. N. R., Ganapathi, L., Vijayaraghavan, R., Rao, G. R., Murthy, K., Mohan Ram, R. A. 1988. *Physica C* 156: 827–33; 1989. *J. Solid State Chem.* 79: 177–80
118. Sheng, Z. Z., Hermann, A. M. 1988. *Nature* 332: 55–57. 138–40
119. Torardi, C. C., Subramanian, M. A., Calabrese, J. C., Gopalakrishnan, J., Morrissey, K. J., et al. 1988. *Science* 240: 631–33
120. Ganguli, A. K., Nanjundaswamy, K. S., Subbanna, G. N., Rajumon, M. K., Sarma, D. D., Rao, C. N. R. 1988. *Mod. Phys. Lett. B* 2: 1169–76
121. Maignan, A., Michel, C., Hervieu, M., Martin, C., Groult, D., Raveau, B. 1988. *Mod. Phys. Lett. B* 2: 681–86; Harvieu, M., Maignan, A., Martin, C., Michel, C., Provost, J., Raveau, B. 1988. *Mod. Phys. Lett. B* 2: 1103–7
122. Ganguli, A. K., Subbana, G. N., Rao, C. N. R. 1988. *Physica C* 156: 181–82
123. Hervieu, M., Maignan, A., Martin, C., Michel, C., Provost, J., Raveau, B. 1988. *J. Solid State Chem.* 75: 212–16
124. Parkin, S. S. P., Lee, V. Y., Nazzal, A. I., Savoy, R., Bayers, R., La Placa, S. J. 1988. *Phys. Rev. Lett.* 61: 750–53
125. Cava, R. J., Batlogg, B., Krajewski, J. J., Rupp, L. W., Schneemeyer, L. F., et al. 1988. *Nature* 336: 221–23
126. Cava, R. J., Batlogg, B., Krajewski, J. J., Farrow, R., Rupp, L. W., et al. 1988. *Nature* 332: 814–16
127. Day, P., Resseinsky, M., Prassides, K., David, W. I. F., Moze, O., Soper, A. 1987. *J. Phys. C* 20: L429–33
128. Johnston, D. C., Jacobson, A. J., Newsam, J. M., Lewandowski, J. T., Goshorn, D. P., et al. 1987. *Symp. Ser.* 351: 136–51
129a. Beech, F., Miraglia, S., Sontoro, A., Roth, R. S. 1987. *Phys. Rev. B* 35: 8778–83
129b. Jorgensen, J. D., Beno, M. A., Hinks, D. G., Soderholm, L., Volin, K. J., et al. 1987. *Phys. Rev. B* 35: 7915–22
130. Karpinski, J., Kaldis, E., Jilek, E., Rusiecki, S., Bucher, B. 1988. *Nature* 336: 660–62
131a. Ganguli, A. K., Nanjundaswamy, K. S., Rao, C. N. R. 1988. *Physica C* 156: 788–90
131b. Subramanian, M. A., Torardi, C. C., Gopalakrishnan, J., Gai, P. L., Calabrese, J. C., Askew, T. R., Flippen, R. B., Sleight, A. W. 1988. *Science* 242: 249–51
132a. Ganguli, A. K., Nagarajan, R., Nanjundaswamy, K. S., Rao, C. N. R. 1989. *Mater. Res. Bull.* 24: 103–7
132b. Rao, C. N. R., Bhat, V., Nagarajan, R., Rao, G. R., Sankar, G. 1989. *Phys. Res. B.* In press
132c. Rao, C. N. R., Ganguli, A. K., Vijayaraghavan, R. 1989. *Phys. Rev. B.* In press
133. Umezawa, A., Crabtree, G. W., Liu, J. Z. 1988. *Physica C* 153–155: 1461–64
134. Batlogg, B., Cava, R. J., Jayaraman, A., van Dover, R. B., Kourouklis, G. A., et al. 1987. *Phys. Rev. Lett.* 58: 2333–36
135. Van Bentum, P. J. M. 1988. *Physica C* 153–155: 1718–25
136a. Bhat, S. V., Ganguly, P., Ramakrishnan, T. V., Rao, C. N. R. 1987. *J. Phys. C* 20: L559–61
136b. Portis, A. M., Blazey, K. W., Muller, K. A., Bednorz, J. G. 1988. *Europhys. Lett.* 5: 487–91
137. Dunlap, B. D., Slaski, M., Hinks, D. G., Soderholm, L., Beno, M., et al. 1987. *J. Magn. Magn. Mater.* 68: L139–45
138. Takahashi, T., Matsuyama, H., Yoshida, H. K., Okabe, Y., Hosoya, S., et al. 1988. *Nature* 334: 691–93
139. Bianconi, A., De Sourtis, M., Flank, A. M., Fontaine, A., Lagarde, P., et al. 1988. *Physica C* 153–155: 1760–65
140a. Sarma, D. D., Ganguly, P., Sreedhar, K., Rao, C. N. R. 1987. *Phys. Rev. B* 37: 2371–73
140b. Sarma, D. D., Rao, C. N. R. 1988. *Solid State Commun.* 65: 47–48
140c. Rao, C. N. R., Sarma, D. D., Rao, G. R. 1989. *Phase Transitions.* In press
141. Fuggle, J. C., Fink, J., Nücker, N. 1988. *Int. J. Mod. Phys. B* 1: 1185–1226
142. Fuggle, J. C., Weijs, P. J. W., Schorl,

R., Sawatzky, G. A., Fink, J., et al. 1988. *Phys. Rev. B* 37: 123–30
143. Chakraverty, B. K., Sarma, D. D., Rao, C. N. R. 1988. *Physica C* 156: 413–17
144. Guo, Y., Langlois, J., Goddard, W. A. III. 1988. *Science* 239: 896–99
145a. Fink, J., Nücker, N., Romberg, H., Fuggle, J. C. 1989. *Phys. Rev.* In press
145b. Himpsel, F. J., Chandrasekhar, G. V., McLean, A. B., Shafer, M. W. 1988. *Phys. Rev. B* 38: 11946–50
146. Sarma, D. D. 1988. *Phys. Rev. B* 37: 7948–52
147. Emery, V. J. 1987. *Phys. Rev. Lett.* 58: 2794–96
148. Hirsch, J. E. 1987. *Phys. Rev. Lett.* 59: 228–31
149a. Takura, Y., Torrance, J. B., Huang, T. C., Nazzal, A. I. 1988. *Phys. Rev. B* 38: 7156–59
149b. Takura, Y., Takagi, H., Uchida, S. 1989. *Nature* 337: 345–47
149c. Rajumon, M. K., Sarma, D. D., Vijayaraghavan, R., Rao, C. N. R. 1989. *Solid State Commun.* 70: 875–77
150. Anderson, P. W. 1987. *Science* 235: 1196–99
151. Zhang, F. C., Rice, T. M. 1987. *Phys. Rev. B* 37: 3759–65
152. Ramakrishnan, T. V., Rao, C. N. R. 1989. *J. Phys. Chem.* In press
153. Schluter, M., Hybertsen, M. S., Christensen, N. E. 1988. *Physica C* 153–155: 1217–22
154. Fujimori, A. 1987. *Phys. Rev. B* 35: 8814–18
155. Eskes, H., Sawatzky, G. A. 1988. *Phys. Rev. Lett.* 61: 1415–17
156. Schrieffer, J. R., Wen, X. G., Zhang, S. C. 1988. *Phys. Rev. Lett.* 60: 944–46
157. Baskaran, G., Zou, Z., Anderson, P. W. 1987. *Solid State Commun.* 63: 973–77
158. Wheatley, J. M., Hsu, T. C., Anderson, P. W. 1988. *Phys. Rev. B* 37: 627–32
159. Burdett, J. K., Kulkarni, G. V., Levin, K. 1987. *Inorg. Chem.* 26: 3650–52
160. Hagenmuller, P., ed. 1972. *Preparative Methods in Solid State Chemistry*. New York: Academic
161. Honig, J. M., Rao, C. N. R., eds. 1981. *Preparation and Characterization of Materials*. New York: Academic
162. Rao, C. N. R., Gopalakrishnan, J. 1987. *Acc. Chem. Res.* 20: 228–35
163a. Ganapathi, L., Ramanan, A., Gopalakrishnan, J., Rao, C. N. R. 1986. *J. Chem. Soc. Chem. Commun.*, pp. 62–63
163b. McCarron, E. W. III. 1986. *J. Chem. Soc. Chem. Commun.*, pp. 336–37
164. Schollhorn, R. 1980. *Angew. Chem. Int. Ed. Engl.* 19: 983–93
165. Whittingham, M. S., Jacobson, A. J., eds. 1982. *Intercalation Chemistry*. New York: Academic
166. Kumada, N., Muramutu, S., Muto, F., Kinomura, N., Kikkawa, S., Koizumi, M. 1988. *J. Solid State Chem.* 73: 33–39
167. Rosique, C., Gonzales, J., Valletregi, M., Alario-Franco, M. A. 1988. *J. Solid State Chem.* 76: 313–18
168. Rice, C. E., Jackel, J. L. 1982. *J. Solid State Chem.* 41: 57–61
169. Cava, R. J., Santoro, A., Murphy, D. W., Zahurak, S., Roth, S. 1982. *J. Solid State Chem.* 42: 251–56
170a. Izawa, H., Kikkawa, S., Koizumi, M. 1987. *J. Solid State Chem.* 69: 336–42
170b. Clearfield, A., Lehto, J. 1988. *J. Solid State Chem.* 73: 98–106
171. Tourmoux, M., Murchand, R., Brohan, L. 1986. *Prog. Solid State Chem.* 17: 33–52
172a. Banks, E., Wold, A. 1974. In *Solid State Chemistry*, ed. C. N. R. Rao. New York: Dekker
172b. McCarroll, W. H., Darling, C., Jakubicki, G. 1983. *J. Solid State Chem.* 48: 189–94
173. Horowitz, H. S., Longo, J. M., Lewandowski, J. T. 1981. *Mater. Res. Bull.* 16: 489–93
174. Sen, A., Chakraverty, D. 1986. *Proc. Indian Natl. Sci. Acad. A* 52: 159–75
175. Nagano, M., Greenblatt, M. 1988. *Solid State Commun.* 67: 595–602
176. Osiko, V. V., Borik, M. A., Lomonova, E. E. 1987. *Annu. Rev. Mater. Sci.* 17: 101–60
177. Joubert, J. C., Chenavas, J. 1975. In *Treatise in Solid State Chemistry*, ed. N. B. Hannay, Vol. 5. New York: Plenum
178. Hagenmuller, P. 1986. *Proc. Indian Natl. Sci. Acad. A* 52: 102–16
179. Rao, C. N. R., Rao, K. J., Gopalakrishnan, J. 1985. *Annual Reports C*. London: Royal Soc. Chem.
180. Cheetham, A. K. 1986. *Proc. Indian Natl. Sci., Acad. A* 52: 25–33; Cheetham, A. K. 1981. In *Non-Stoichiometric Oxides*, ed. O. T. Sorenseon. New York: Academic
181. Cox, D. E., Hastings, J. B., Thomlinson, W., Prewitt, C. 1983. *Nucl. Instrum. Methods* 208: 573–78
182. Johnson, M. W., David, W. I. F. 1985. *Rutherford-Appleton Lab. Rep.* N. 85/112
183. Altfield, J. P., Sleight, A. W., Cheetham, A. K. 1986. *Nature* 322: 620–22
184. Cheetham, A. K., David, W. I. F., Eddy, M. M., Jakeman, R. J. B., Johnson, M. W., Torardi, C. C. 1986. *Nature* 320: 46–48

185. Loong, C. K. 1985. *J. Appl. Phys.* 57: 3772–78
186a. Jefferson, D. A. 1982. *Philos. Trans. R. Soc. London Ser. A* 305: 535–44
186b. Cheetham, A. K., Skarnulis, A. J. 1981. *Anal. Chem.* 53: 1060–64
186c. Egerton, R. F. 1982. *Philos. Trans. R. Soc. London Ser. A* 305: 521–30
187. Rao, C. N. R., Sparrow, T. G., Williams, B. G., Thomas, J. M. 1984. *J. Chem. Soc. Chem. Commun.*, pp. 1238–40
188. Williams, B. G. 1987. *Prog. Solid State Chem.* 17: 87–143
189a. Rao, C. N. R., Sarma, D. D. 1982. *J. Solid State Chem.* 45: 14–28
189b. Rao, C. N. R. 1986. *Philos. Trans. R. Soc. London Ser. A* 318: 37–50
189c. Reviere, J. C. 1982. *Philos. Trans. R. Soc. London Ser A* 305: 545–55
190a. Binnig, G., Rohrer, H. 1984. *Physica B* 127: 37–45
190b. Tersoff, J., Hamann, D. R. 1985. *Phys. Rev. B* 31: 805–12
191. Hinks, D. G., Richards, D. R., Dabrowski, B., Marx, D. T., Mitchell, A. W. 1988. *Nature* 335: 419–21
192. Uemura, Y. J., Sternlieb, B. J., Cox, D. E., Brewer, J. H., Kadono, R., et al. 1988. *Nature* 335: 151–53
193. Rao, C. N. R., Ganguly, P., Hegde, M. S., Sarma, D. D. 1987. *J. Am. Chem. Soc.* 109: 6893–94
194. Shafer, M. W., Penney, T., Olson, B. L. 1987. *Phys. Rev. B* 36: 4047–50
195. Dai, Y., Manthiram, A., Campion, A., Goodenough, J. B. 1988. *Phys. Rev. B* 38: 5091–93